



**University of
Zurich**^{UZH}

Evapotranspiration and Water Use Efficiency in Agricultural Areas: Creating a new Tool using Remote Sensing to Help Farmers reduce Water Losses

ESS 511 Master's Thesis

Author

Jasmin Kesselring
12-737-458

Supervised by

Dr. Eugénie Paul-Limoges
Prof. Dr. Alexander Damm

Faculty representative

Prof. Dr. Alexander Damm

29.09.2020

Department of Geography, University of Zurich



**University of
Zurich^{UZH}**

ESS 511
Master Thesis
29. September 2020

Evapotranspiration and Water Use Efficiency in Agricultural Areas

**Creating a new Tool using Remote Sensing to help Farmers reduce
Water Losses**

Jasmin KESSELRING
12-737-458

Supervised by:
Dr. Eugénie PAUL-LIMOGES
Prof. Dr. Alexander DAMM-REISER

Faculty representative:
Prof. Dr. Alexander DAMM-REISER

Remote Sensing Laboratories
Department of Geography
University of Zurich

Abstract

Up to 70% of the available fresh water is used in agriculture. As the occurrence of droughts in combination with the demand for water are steadily rising, water will become an increasingly scarce resource for both food production and drinking. To prevent shortcomings in food production, an effective water use monitoring is necessary to increase water use efficiency and reach a sustainable water management for the future. Although some scientific methods exist to monitor water use on agricultural lands, there is generally a communication gap between scientists and the people, here the farmers, who are meant to implement the findings in their daily work. The aim of this thesis is to support farmers in their decision making and water management by making remotely sensed products to monitor agricultural water use accessible through performance indicators. With evapotranspiration calculated using the Penman-Monteith equation, and gross primary production with the light use efficiency approach, the water use efficiency of different agricultural fields was modelled using Sentinel-2 data. The modelled parameters were compared to in situ measurements of the eddy flux tower at the study site in Oensingen, Switzerland, to verify the reliability of the generated base maps. Using a multi-temporal data stack of three indices (leaf area index, chlorophyll vegetation index, green leaf index), the fields in the study area were classified into three crop types (summer, winter and mixed crops). Using these three classes and the previously calculated parameters, three performance indicators (yield, water use and productivity) were developed and implemented into an interactive R Shiny application, so that farmers can monitor the water use of their fields. Despite the limitations of the used methods, especially the classification approach, the development of performance indicators and creation of an application in R Shiny to simplify complex remote sensing data proved to be very promising. With ongoing research in both the calculation of the input parameters and the classification of agricultural fields, the results of the performance indicators could be improved to make it a reliable tool for farmers.

Contents

Abstract	III
List of Figures	VII
List of Tables	IX
1 Introduction	1
2 Material and Methods	5
2.1 Study Area	5
2.2 Remote Sensing Data	5
2.2.1 Satellite Spectroscopy Data	5
2.2.2 Airborne Spectroscopy Data	7
2.2.3 Field Spectroscopy Data	7
2.3 Meteorological Data	7
2.3.1 Meteo Station Oensingen	7
2.3.2 Meteo Station Wynau	8
2.4 Working Process	8
2.5 Classification of Test Fields	8
2.5.1 Leaf Area Index	9
2.5.2 Chlorophyll Vegetation Index	9
2.5.3 Green Leaf Index	10
2.5.4 Classification using the Spectral Angle Mapper	10
2.6 Evapotranspiration	11
2.6.1 The Penman-Monteith Equation	11
2.6.2 Input Parameters for the Penman-Monteith Equation	12
2.6.2.1 Psychrometric Constant γ	13
2.6.2.2 Mean Air Density ρ_a	13
2.6.2.3 Vapour Pressure of saturated Air e_s	13
2.6.2.4 Actual Vapour Pressure e_a	14
2.6.2.5 Slope of Vapour Pressure Curve Δ	14
2.6.2.6 Aerodynamic Resistance r_a	14
2.6.2.7 Surface Resistance r_s	15
2.6.2.8 Net Radiation R_n	16
2.6.2.9 Ground Heat Flux G	16
2.7 Gross Primary Production	17

2.7.1	Photosynthetically Active Radiation	17
2.7.2	Fraction of absorbed PAR	18
2.7.3	Light Use Efficiency	18
2.8	Water Use Efficiency	18
2.9	Performance Indicators	19
2.9.1	Yield	19
2.9.2	Water	19
2.9.3	Productivity	19
3	Results	21
3.1	Classification of the Study Area into Crop Types	21
3.2	Calculation of the Base Maps	21
3.2.1	Leaf Area Index Values	21
3.2.2	Evapotranspiration Values	24
3.2.3	Gross Primary Production Values	26
3.2.4	Water Use Efficiency Values	29
3.3	Performance Indicators	32
3.3.1	Yield	34
3.3.2	Water Use	34
3.3.3	Productivity	37
4	Discussion	39
4.1	Interpretation of the Classification	39
4.2	Reliability of the Base Maps	40
4.2.1	Leaf Area Index Base Map	40
4.2.2	Evapotranspiration Base Map	40
4.2.3	Gross Primary Production Base Map	42
4.2.4	Water Use Efficiency Base Map	43
4.3	Added Value of the Performance Indicators	44
4.4	Outlook	45
4.4.1	Advancement of Base Maps	45
4.4.2	Making the App more efficient	46
5	Conclusion	47
	Bibliography	49
	A Appendix - Additional Figures and Tables	57
	Acknowledgements	59
	Personal Declaration	61

List of Figures

2.1	Map of the study area with the location of the six test fields and meteorological stations.	6
2.2	Flow chart of the working process.	9
2.3	Leaf area index, green leaf index and chlorophyll vegetation index over the year 2019 in six different test fields.	11
2.4	Spectrum of solar radiation on Earth.	17
3.1	Map of the three crop type classes in the study area using the spectral angle mapper algorithm for classification.	22
3.2	Daily mean leaf area index values for the whole study area and the three crop classes.	23
3.3	Heat map of daily mean leaf area index values over the whole study area on June 19 th 2019.	23
3.4	Mean hourly evapotranspiration of all eleven days in the study period.	24
3.5	Daily evapotranspiration of the whole study area and the three crop classes.	25
3.6	Heat map of mean daily evapotranspiration over the whole study area on June 19 th 2019.	25
3.7	Comparison of evapotranspiration from flux tower and in situ data as line and scatter plot.	26
3.8	Mean hourly gross primary production of all days in the study period.	27
3.9	Daily gross primary production of the whole study area and the three crop classes.	27
3.10	Heat map of daily mean gross primary production over the whole study area on June 19 th 2019.	28
3.11	Comparison of gross primary production from flux tower and in situ data as line and scatter plot.	29
3.12	Mean hourly water use efficiency of all days in the study period	30
3.13	Daily mean water use efficiency of the whole study area and the three crop classes.	31
3.14	Heat map of daily mean water use efficiency over the whole study area on June 19 th 2019.	31
3.15	Start page of the R Shiny app.	32
3.16	Daily gross primary production of field 3 displayed in the app.	33
3.17	Adaptable graphics for the yield performance indicator.	34
3.18	Possible yield of field 3 displayed in the app.	35
3.19	Adaptable graphics for the water performance indicator.	36
3.20	Possible water savings of field 3 displayed in the app.	36
3.21	Adaptable graphics for the productivity performance indicator.	37

3.22	Productivity of field 3 displayed in the app.	38
A.1	Daily mean leaf area index, evapotranspiration, gross primary production and water use efficiency of the six test fields	58

List of Tables

2.1	Sentinel-2 bands, spectral and spatial resolution, together with the weighing coefficients used for the albedo calculation.	6
2.2	Acquisition times of the Sentinel-2 tiles used.	7
2.3	Meteorological measurement specifications at the stations in Oensingen and Wynau.	8
3.1	Performance indicator categories of the six test fields when compared to their respective crop class.	38
A.1	Daily mean leaf area index for all classes and test fields.	57
A.2	Daily mean evapotranspiration for all classes and test fields.	57
A.3	Daily mean gross primary production for all classes and test fields.	57
A.4	Daily mean water use efficiency for all classes and test fields.	58

1 Introduction

A large proportion of the available fresh water on earth is used for irrigation in agriculture (Rosegrant et al., 2009). In drought-prone regions, agricultural water use can account up to 70% of the available fresh water (WWAP, 2014). With climate models predicting warmer and drier summers in the near future (Falloon & Betts, 2010; Hegerl et al., 2007), the occurrence and severity of droughts in Europe are likely to increase (Fisher et al., 2017; Lehner et al., 2006). Water consumption for use in the energy and agriculture sectors will also increase in the near future, mostly due to population growth (Jewell, 2011). And with this, distribution problems of fresh water between all interested parties will become more complex (Veetil & Mishra, 2016). This could lead to shortages in the availability of fresh water resources for agricultural use (Falloon & Betts, 2010; Fisher et al., 2008) and, thus, to shortcomings in food production. Therefore, an efficient irrigation technique and schedule is needed to increase water use efficiency and to attain a sustainable water management in the future (Farg et al., 2017). Additionally, knowledge regarding the vulnerability and availability of fresh water will help to prevent water shortages not only in agriculture (Veetil & Mishra, 2016), but in other ecosystems as well.

The concept of green and blue water can help in understanding the scarcity and vulnerability of water and which parts of the water cycle are affected by the overuse of water for agricultural purposes. All fresh water on the surface of the Earth originates from rainfall and will eventually enter the ocean. The water can either take the path of blue water, which is readily available surface water in lakes and aquifers (Falkenmark, 2013; Rodrigues et al., 2014) or the path of green water which is described as the sum of evapotranspiration and soil water content as storage (Schuol et al., 2008). In other words, the rain water is stored in unsaturated soil and vegetation (Veetil & Mishra, 2016). Even if 3/5 of the precipitation takes the path of green water (Oki & Kanae, 2006), the indirectness of the probable water scarcity makes it invisible to economy and difficult to quantify (Schyns et al., 2015). However, green water is very important for terrestrial ecosystems as plant growth is a function of soil moisture, hence, it is responsible for the production of food (Falkenmark, 2013). During the growing season of plants, the global consumption of green water can amount up to 84% (Lui & Yang, 2010). As the availability of green water is limited (Schyns et al., 2015), overuse effects can occur. These effects are not as easy to quantify as blue water scarcity effects, as they are only detectable indirectly in the inability of plants to grow. In times when the natural green water is scarce, agriculture uses blue water to irrigate crops (Schyns et al., 2015), which can lead to a blue water scarcity if the drought occurs over a long period of time.

As crop water deficits depend on the water availability in the root zone and are, therefore, difficult for farmers to detect above the soil surface (Chartzoulakis & Bertaki, 2015), agricultural fields are often over-irrigated (Chartzoulakis & Bertaki, 2015). Not only can the overuse of water

diminish the quantity of available blue water (Rosegrant et al., 2009), it can also have negative effects on the agricultural fields themselves. For instance, the loss of nutrients, mostly nitrogen due to leaching, can pollute ground and surface water (Velthof et al., 2014). The decreased nutrient source can then lead to yield losses in farming (Riley et al., 2001). Irrigation can also cause an increased salinity of the soil which can induce both land and water degradation (Chartzoulakis & Bertaki, 2015; Chhabra, 1996; Rosegrant et al., 2009). To remedy the multiple negative effects of over-irrigation, water and nitrogen use needs to be more efficient in the future (Kodur et al., 2019). This can be achieved by minimizing the water loss, and increasing Water Use Efficiency (WUE) and irrigation, which has little to no effect on the crop yield. This principle is called deficit irrigation (Karam et al., 2007). It helps to achieve the maximum yield and reduce negative effects such as nutrient leaching into the soil and ground water (Irmak et al., 2016). However, WUE does not solely depend on the irrigation of the field, it also depends on environmental influences (Mo et al., 2005).

Multiple research projects have studied WUE of different crops and grasslands using field methods and models (Karam et al., 2007; Tian et al., 2010). This has led to very good results on a small spatial scale. To be able to assess the WUE on a bigger scale and over longer time periods another technique has to be used. Remote sensing can provide systematic and consistent observations and as it is available globally, it can be used for crop monitoring on large scales (Wolanin et al., 2019). Additionally, remote sensing data has mostly the same spatial density all over the world and the measurements are repeatable without additional effort (Mo et al., 2005). Further, data, such as used in this study from the European Space Agency satellite Sentinel-2, are open source and can be downloaded and processed by every interested person. The gathered data can be used for crop yield forecasting and management decision optimisation (Wolanin et al., 2019). The local data can be used to describe key ecosystem functions which can then be scaled up to a global extent using this technique (Masek et al., 2015). Both Evapotranspiration (ET) and Gross Primary Production (GPP) are important parameters in local and regional water management plans and can be modeled using remote sensing approaches. Based on these two products, the WUE can be calculated for the desired region which can then be used for irrigation schedules and with some interpretation for the prediction of long-term effects of land use changes (Glenn et al., 2007). However, most results of scientific publications are too abstract to be implemented directly by the end-user. There is a transfer and knowledge gap between the scientists and the people, here the farmers, who are meant to implement the findings in their daily work.

The aim of this thesis is to support farmers in their decision making and water management by making remotely sensed products to monitor water use by plants (such as ET, GPP and WUE) accessible through performance indicators. Hence, our research questions are formulated accordingly:

1. Which parameters and data comparisons can be useful to farmers in their decision making?
2. How can abstract remote sensing data be presented and visualised, so that the information is usable by the target group?

As most farmers are not familiar with remote sensing data, we expect an increase in the usability of the product, if the output data is presented in an understandable context. To achieve the aim of the thesis and to answer the research questions, ET is modelled using the Penman-Monteith equation and GPP is calculated with the light use efficiency approach. Using the output of these two parameters, WUE can be estimated. With the results of all these calculations three performance indicators are developed which can be accessed via a user-friendly application.

2 Material and Methods

2.1 Study Area

The cropland site in Oensingen (SO), Switzerland, has been part of the Swiss FluxNet since 2004 and is thus, equipped with an eddy covariance flux tower and a meteorological station (Paul-Limoges et al., 2018). The site (47°17'11.1" N, 7°44'01.5" E, 452 m a.s.l.) is an agricultural field with a rotation of different crop types over the years, such as peas, sugar beet, and winter barley (Damm et al., 2015). Tower-based hyperspectral measurements were made at the site with a high precision spectrometer (UniSpec-DC) from 2015 to 2018 (Paul-Limoges et al., 2018) and with a fluorescence box (FloX-Box) since April 2019. For this thesis a slightly larger study area was used, instead of only the test fields in Oensingen. An area reaching from Wiedlisbach (BE) in the south-west to Egerkingen (SO) in the north-east was chosen (Figure 2.1). This way, the behaviour of multiple crop types and agricultural fields can be compared.

2.2 Remote Sensing Data

In this study we analyzed eleven Sentinel-2 scenes from April to October 2019. Additionally, APEX scenes were used to help classify the test fields into different categories. FloX-Box measurements were used for the net radiation calculation within the Penman-Monteith equation (see 2.6.2.8).

2.2.1 Satellite Spectroscopy Data

The Sentinel-2 mission of the European Space Agency (ESA) provides data from two satellites Sentinel-2A (since June 2015) and Sentinel-2B (since March 2017) with a high temporal resolution, due to the revisiting period of 5 days (Drusch et al., 2012). Its Multi-Spectral Instrument (MSI) samples in 13 spectral bands from visual to shortwave infrared (Wolanin et al., 2019). Depending on the spectral band the spatial resolution varies between 10 – 60 m (Drusch et al., 2012) (Table 2.1). In this thesis Level-2A data was used. This product provides bottom of atmosphere reflectance data composed of 100 km² tiles in cartographic geometry (UTM/WGS84 projection) (ESA, 2015). Eleven cloud-free scenes (tile T32TMT) from April to October 2019 were selected to cover the growing season of most agricultural crops present in the study area (Table 2.2). The selected scenes were then cut to a spatial subset of the study area (WGS84 NW-corner: 47.32N 7.61E; SE-corner: 47.26N 7.82E) and resampled to 10 m resolution based on band 2 using the Sentinel Application Platform (SNAP).



FIGURE 2.1: Study area of the cropland site in Oensingen (SO), Switzerland, in colour. With the six selected test fields marked in yellow and the meteorological stations Oensingen and Wynau as triangles. The Sentinel-2 scene of June 19th 2019 was used as background.

TABLE 2.1: Thirteen bands of ESA’s Sentinel-2 satellite with the spectral resolution shown as the center wavelength of the band and the spatial resolution in meters. The weighing coefficients ω_{bi} according to (Vanino et al., 2018) are used for the albedo calculation (Eq. 2.18).

Band Number	Center Wavelength (nm)	Spatial Resolution (m)	ω_{bi} (-)
1	443	60	
2	490	10	0.1324
3	560	10	0.1269
4	665	10	0.1051
5	705	20	0.0971
6	740	20	0.0890
7	783	20	0.0818
8	842	10	0.0722
8a	865	20	-
9	940	60	-
10	1375	60	-
11	1610	20	0.0167
12	2190	20	0.0002

TABLE 2.2: Acquisition dates and times of the eleven T32TMT Sentinel-2 tiles used.

Acquisition Date (Date)	Acquisition Time (UTC)
20/04/2019	10:30:31
04/06/2019	10:30:29
19/06/2019	10:30:31
29/06/2019	10:30:31
04/07/2019	10:30:29
24/07/2019	10:30:29
08/08/2019	10:30:31
18/08/2019	10:30:31
28/08/2019	10:30:21
12/09/2019	10:30:19
12/19/2019	10:30:29

2.2.2 Airborne Spectroscopy Data

The Airborne Prism Experiment (APEX) is a push-broom imaging spectrometer with a spectral range from 400 nm to 2500 nm (Schaepman et al., 2015). The data set includes 313 spectral bands in a 2 m spatial resolution. The images in the Oensingen region were taken on June 7th, July 25th and 30th 2019. This data was not used in any calculations but to visually classify the different crops on the test fields, as this was difficult with the lower resolution of the Sentinel-2 scenes.

2.2.3 Field Spectroscopy Data

The Fluorescence Box (FloX-Box) manufactured by JB-Hyperspectral, Germany, situated next to the eddy flux tower at the Oensingen test site is primarily used to measure sun induced fluorescence. For this thesis the spectral radiance measurements [$\text{W m}^{-2} \text{sr}^{-1} \text{nm}^{-1}$] were used. From this data the daily mean and hourly mean values of the selected dates were calculated.

2.3 Meteorological Data

Multiple meteorological parameters are necessary input arguments for the Penman-Monteith equation. The data was provided by two different meteorological stations in the study area (Table 2.3).

2.3.1 Meteo Station Oensingen

The measurement equipment of the meteo station is situated next to the eddy flux tower at the Oensingen test site (47°17'11.1" N, 7°44'01.5" E, 452 m a.s.l.). Air temperature, relative humidity, atmospheric pressure and scalar wind speed data was used from this station in the ET calculation. All data has a temporal resolution of 30 minutes. The data was provided by the ETH grassland sciences group ('Grassland Sciences', 2020).

2.3.2 Meteo Station Wynau

The meteo station in Wynau (47°15'18.124" N, 7°47'14.889" E, 422 m a.s.l.) is operated by Meteo-Swiss. The global radiation measurements were used in the gross primary production calculation, namely in the estimation of the photosynthetically active radiation (PAR) (see 2.7.1). These data has a temporal resolution of 10 minutes. From that, a daily and hourly mean value of the selected dates was calculated. The meteo data was accessed using IDAWEB, the data platform of the MeteoSwiss services and have also been provided by MeteoSwiss, the Swiss Federal Office of Meteorology and Climatology.

TABLE 2.3: Meteorological measurement specifications with unit, temporal resolution and height and model of the instrument.

Parameter	Unit	Temporal Resolution	Measurement Height	Measurements Device	Meteorological Station
BOA Irradiance (400.23 – 900.54 nm)	$W m^{-2} nm^{-1} sr^{-1}$	ms (UTC)	2 m	FloX-Box by JB-Hyperspectral, Germany	Oensingen
Temperature	C	30 min. (GMT +1)	2 m	Rotronic MP101A, Bassersdorf, Switzerland	Oensingen
Atm. pressure	Pa	30 min. (GMT +1)	1 m	-	Oensingen
Windspeed	$m s^{-1}$	30 min. (GMT +1)	2 m	Cup anemometer	Oensingen
Rel. humidity	%	30 min. (GMT +1)	2 m	Rotronic MP101A, Bassersdorf, Switzerland	Oensingen
Global radiation	$W m^{-2}$	10 min. (UTC)	2 m	Pyranometer CM21 by Kipp & Zonen	Wynau

2.4 Working Process

As can be seen in Figure 2.2, the programs Excel and SNAP were used for pre-processing. For all calculations in the processing part of the thesis the software MATLAB (version R2019b) was used. The performance indicators were calculated and visualised in R Shiny (RStudio, 2020) and the base maps of the parameters were created in QGIS (version 3.10.2).

2.5 Classification of Test Fields

The classification of the fields into different crop types was necessary to be able to compare the selected test fields to similar fields in the study area. In a first step, the study area, which only consists of agricultural fields, had to be separated from the rest of the Sentinel-2 scene, otherwise the fields would be compared to the forest or urban area within the region. For this polygon masking in QGIS was used. In a second step, three indices were selected, which can explain different plant traits and hence, behave differently for different field types. Sections 2.5.1 – 2.5.3 describe the indices used. In a third step, six test fields were selected (Figure 2.1), which should simulate the input of an actual farmer to the later created performance indicator app. The fields were selected due to their different appearance in the RGB representation of the Sentinel-2 scenes and were of homogeneous structure. Field 4 was selected as it is the location of the measurement devices of the Oensingen meteo station. The fields are represented by the mean of values of a

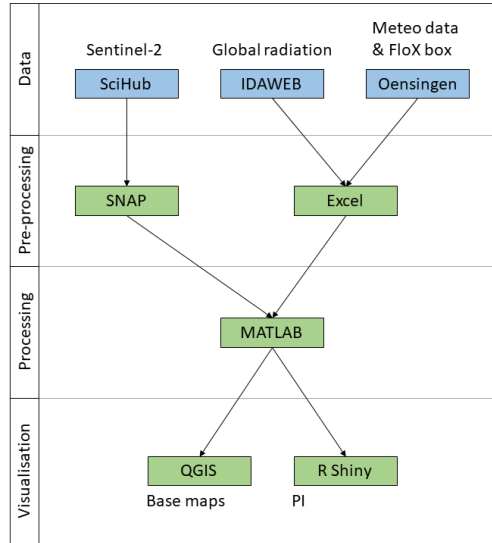


FIGURE 2.2: Flow chart of the working process with the sources of the data and the computer programs used in the different steps of the thesis indicated.

square of around 100 pixels in the middle of the fields. The position of the pixels was extracted using SNAP.

2.5.1 Leaf Area Index

The LAI describes the degree of the canopy development (Vincini et al., 2008) and the leaf architecture (Glenn et al., 2007). With this index the potential surface for photosynthesis and leaf gas exchange is calculated (Viña et al., 2011). The formula for the calculation of the LAI can be seen under section 2.6.2.7. As the LAI is used to estimate ET, the classification cannot simply be based on this index. Otherwise a bias would occur. Hence, two other indices were chosen.

2.5.2 Chlorophyll Vegetation Index

The chlorophyll vegetation index (CVI) is a vegetation index which can be used to estimate the photosynthetic capacity and productivity of a plant canopy (Vincini et al., 2008). This index relies on the assumption that the leaf chlorophyll content is no longer influenced by the LAI when the canopy is closed (Vincini et al., 2008). The CVI was calculated according to Vincini et al. (2008) using the Sentinel-2 bands 3, 4 and 8.

$$CVI = \frac{R_n \cdot R_r}{R_g^2} \quad (2.1)$$

R_g : Band 3 (green) of Sentinel-2 (560 nm)

R_r : Band 4 (red) of Sentinel-2 (665 nm)

R_n : Band 8 (near infrared) of Sentinel-2 (842 nm)

2.5.3 Green Leaf Index

As a third indicator the green leaf index (GLI) was chosen as only bands in the visual range of the spectrum are necessary for the calculation (Hunt et al., 2012). The negative numbers when calculating this index stand for the soil and nonliving surfaces and the positive values are the green leaves and stems of the plants (Louhaichi et al., 2001). To calculate the GLI the method of Louhaichi et al. (2001) was used.

$$GLI = \frac{2 \cdot R_g - R_r - R_b}{2 \cdot R_g + R_r + R_b} \quad (2.2)$$

R_b : Band 2 (blue) of Sentinel-2 (490 nm)

R_g : Band 3 (green) of Sentinel-2 (560 nm)

R_r : Band 4 (red) of Sentinel-2 (665 nm)

2.5.4 Classification using the Spectral Angle Mapper

After looking at the variations in the indices over the course of the study time span, three dates were selected (4th of June, 4th of July and 12th of September), where the indices of the six test fields showed the highest differences (Figure 2.3). The resulting nine images were composed into a layer stack, this way a multi-temporal data set was created. Using this data set, a supervised classification using regions of interest, according to similar colours in the multi-temporal image, was carried out. The Sentinel-2 images, on which all three indices are based, are acquired around the same time during the day (Table 2.2) over the course of the study time. But as the sun angle changes over the year, the illumination of the study area is not the same for the three selected dates. As the spectral angle mapper (SAM) algorithm by Kruse et al. (1993) is independent of the illumination of the scene (Lillesand et al., 2015), this classifier was chosen for the classification. With this algorithm a spectral angle is used to determine the similarity of the image pixel spectrum and a reference spectrum (Weyermann et al., 2009). The classification was performed with ENVI. The three classes were used to generate binary masks to be able to calculate the class means of the ET, GPP and WUE. This way it was possible to compare the selected test field to the mean of the other fields in the area within the same class and hence similar properties.

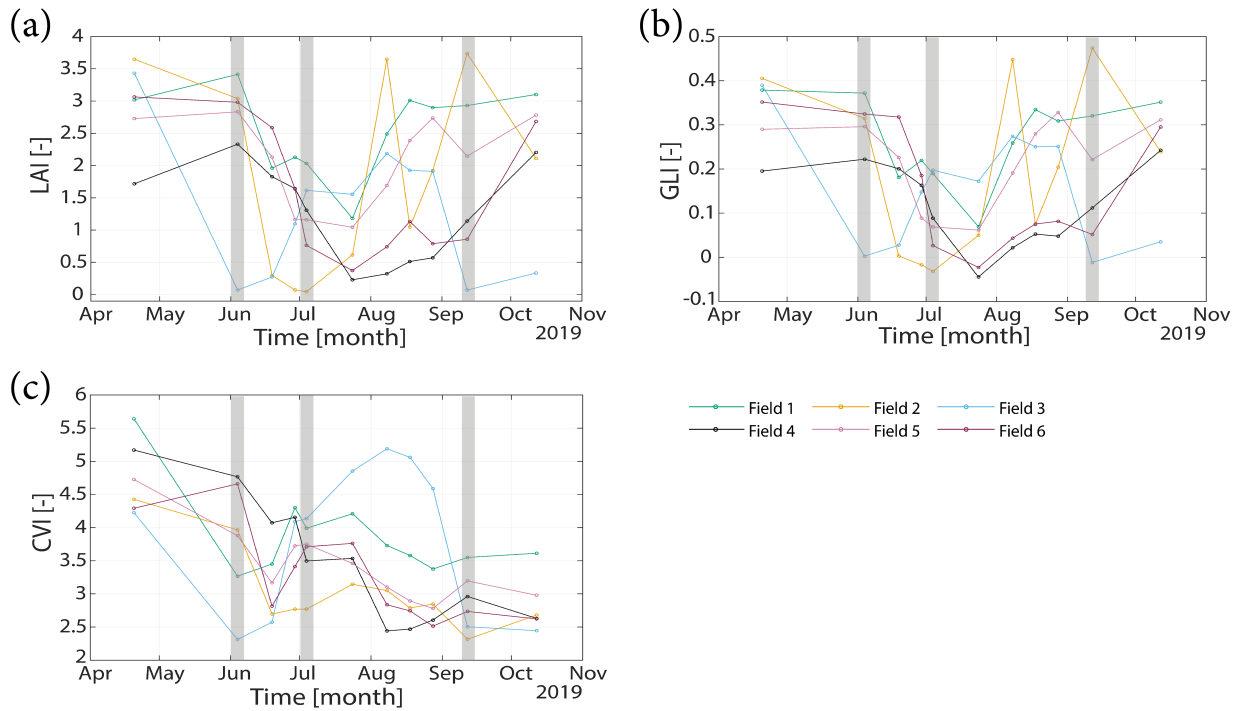


FIGURE 2.3: Calculated indices (a) leaf area index, (b) green leaf index and (c) chlorophyll vegetation index for the six test fields over the year 2019. The grey boxes indicate the dates used for the classification.

2.6 Evapotranspiration

Evapotranspiration (ET) cannot be measured directly from space using satellite data but has to be derived and approximated as an energy variable. For this, multiple types of in situ measurements and information on phenology and vegetation cover are necessary to make sure that the processes are captured correctly within the result (Fisher et al., 2017). To compute real-time ET, a prediction of the daily reference evapotranspiration (ET_0) has to be made. This value is then used as the basis to estimate the crop evapotranspiration and the crop irrigation requirements (Allen 1998). Multiple approaches to calculate ET_0 have been developed over the past half century, all of them using different climatic variables (R. G. Allen et al., 1998). Empirical approaches such as the Primault method are mostly used for practical studies. For instance the MeteoSwiss net uses this method for their measurements (Calanca et al., 2011). The Penman-Monteith approach is, however, the one method recommended by the Food and Agriculture Organisation (FAO) to use for modelling approaches and should be used as sole ET_0 (R. Allen et al., 1994; Calanca et al., 2011). Hence this method is used for this thesis.

2.6.1 The Penman-Monteith Equation

In May 1990, the FAO decided that the Penman-Monteith (P-M) model should be the new standard to estimate ET_0 (de Carvalho et al., 2013). Several different approaches are still used in science, but the P-M model shows the most precise results compared to other models (Garcia et al., 2004; Gavilán et al., 2006). The following P-M equation (Eq. 2.3) describes the ET as a latent heat flux. In

order to be able to evaporate water, energy is necessary, which is provided by the solar radiation term ($R_n - G$, Sections 2.6.2.8 and 2.6.2.9). The amount of water which can be evaporated firstly depends on the difference in pressure in the atmosphere and plant (multiple variables calculated with mostly meteorological data) and secondly on specific plant properties, namely the number and functionality of the stomata openings (r_s , Section 2.6.2.7).

$$ET = \frac{\Delta(R_n - G) + \rho_a C_p \left(\frac{e_s - e_a}{r_a} \right)}{\Delta + \gamma \left(1 + \left(\frac{r_s}{r_a} \right) \right)} \quad (2.3)$$

ET: Evapotranspiration [$\text{mm H}_2\text{O day}^{-1}$]

R_n : Net radiation at crop surface [$\text{MJ m}^{-2} \text{day}^{-1}$]

G: Ground heat flux [$\text{MJ m}^{-2} \text{day}^{-1}$]

e_s : Vapour pressure of the air at saturation [kPa]

e_a : Actual vapour pressure [kPa]

$(e_s - e_a)$: Saturation vapour pressure deficit [kPa]

Δ : Slope of vapour pressure curve [$\text{kPa } ^\circ\text{C}^{-1}$]

γ : Psychrometric constant [$\text{kPa } ^\circ\text{C}^{-1}$]

C_p : Specific heat of the air [$\text{MJ } ^\circ\text{C}^{-1} \text{kg}^{-1}$]

ρ_a : Mean air density at constant pressure [kg m^{-3}]

r_a : Aerodynamic resistance [s m^{-1}]

r_s : Surface resistance [s m^{-1}]

The comparison between ET_0 computed using the P-M equation (Eq. 2.3) and values estimated from weather forecasts show best results in humid areas. The estimation in arid areas can be biased especially during dry periods. This leads to an underestimation of ET most likely due to an overestimation of e_a (Cai et al., 2007). This needs to be considered, in particular if drought events are studied.

2.6.2 Input Parameters for the Penman-Monteith Equation

Most of the components for the P-M equation (Eq. 2.3) have to be calculated or estimated with other parameters as they cannot be measured directly or are dependent on other variables. In this subsection the calculation and data origin of all input parameters will be discussed. The meteorological parameters are assumed constant over the whole study area. ET was calculated firstly as hourly means for each of the eleven days. Secondly, daily mean values were calculated by summing the results of the hourly means. Hence, two different means had to be calculated for each input parameter, a series of hourly means and eleven daily means. The original temporal resolution of the measurements can be seen in Table 2.3. All input parameters for the P-M equation were calculated according to the guidelines of Allen et al. (1998).

2.6.2.1 Psychrometric Constant γ

The psychrometric constant is only dependent on the atmospheric pressure P, which was measured at the Oensingen meteo station.

$$\gamma = \frac{C_p \cdot P}{\epsilon \cdot \lambda} = \frac{1.013 \cdot 10^{-3} \cdot P}{0.622 \cdot 2.45} = 0.6647 \cdot 10^{-3} \cdot P \quad (2.4)$$

γ : Psychrometric constant [kPa °C⁻¹]

C_p : Specific heat of the air = 1.013 · 10⁻³ MJ °C⁻¹ kg⁻¹

P: Atmospheric pressure [kPa]

ϵ : Ratio of molecular weight of water vapour/dry air = 0.622 [-]

λ : Latent heat of vaporisation = 2.45 MJ kg⁻¹

2.6.2.2 Mean Air Density ρ_a

The mean air density is a parameter that is dependent on the atmospheric pressure and indirectly on the air temperature.

$$\rho_a = \frac{P}{T_{kv} \cdot R} = \frac{P}{1.01 \cdot (T + 273) \cdot 0.287} \quad (2.5)$$

ρ_a : Mean air density at constant pressure [kg m⁻³]

P: Atmospheric pressure [kPa]

T_{kv} : Virtual temperature

R: Specific gas constant = 0.287 kJ kg⁻¹ K⁻¹

2.6.2.3 Vapour Pressure of saturated Air e_s

For the estimation of the vapour pressure of saturated air the saturation vapour pressure at air temperature has to be calculated first using equation (Eq. 2.7).

$$e_s = e^\circ(T) \quad (2.6)$$

$$e^\circ(T) = 0.6108 \cdot e^{\left(\frac{17.27 \cdot T}{T + 237.3}\right)} \quad (2.7)$$

e_s : Vapour pressure of saturated air [kPa]

$e^\circ(T)$: Saturation vapour pressure at air temperature T [kPa]

T: Air temperature [°C]

2.6.2.4 Actual Vapour Pressure e_a

The e_a is dependent on the e_s (Eq. 2.6) and the relative humidity of the air. For the daily and hourly e_a equation (Eq. 2.6) both the mean relative humidity and indirectly the mean temperature of the time span have to be considered.

$$e_a = e_s \cdot \frac{RH}{100} \quad (2.8)$$

e_a : Actual vapour pressure [kPa]

RH: Relative humidity [%]

2.6.2.5 Slope of Vapour Pressure Curve Δ

The slope of the vapour pressure curve is the derivative of e_s and T. The second part of the equation (Eq. 2.9) is a simplification of this derivative. For both temperature and e_s the daily and hourly mean have to be taken into consideration.

$$\Delta = \frac{de_s}{dT} = \frac{4098 \cdot [0.6108 \cdot e^{\left(\frac{17.27 \cdot T}{T+237.3}\right)}]}{(T+237.3)^2} \quad (2.9)$$

Δ : Slope of vapour pressure curve [kPa °C⁻¹]

e_s : Vapour pressure of the air at saturation [kPa]

T: Air temperature [°C]

2.6.2.6 Aerodynamic Resistance r_a

The aerodynamic resistance mainly describes the measurement set-up of the wind and humidity parameters and the interaction of these with the plants. Different wind speed averages have to be calculated.

$$r_a = \frac{\ln\left(\frac{z_m-d}{z_{om}}\right) \cdot \ln\left(\frac{z_h-d}{z_{oh}}\right)}{k^2 \cdot u_z} \quad (2.10)$$

r_a : Aerodynamic resistance [s m⁻¹]

z_m : Height of the wind measurements [m]

z_h : Height of the humidity measurements [m]

d: Zero plane displacement height [m]

z_{om} : Roughness length governing momentum transfer [m]

z_{oh} : Roughness length governing transfer of heat and vapour [m]

k = Karman's constant = 0.41 [-]

u_z : Wind speed at height z [m s⁻¹]

The height of the wind and humidity measurements can be found in Table 2.3. The following equations 2.11 – 2.13 show the calculation for parameters additionally needed for equation 2.10.

$$d = \frac{2}{3} \cdot h_c \quad (2.11)$$

$$z_{om} = 0.123 \cdot h_c \quad (2.12)$$

$$z_{oh} = 0.1 \cdot z_{om} \quad (2.13)$$

The FAO suggests a standard height of crops h_c of 0.12 m. This height is further used to calculate d (Eq. 2.11), z_{om} (Eq. 2.12) and indirectly the z_{oh} (Eq. 2.13). Through the assumed constant height over the whole study area an error is induced to the result of the ET calculation.

2.6.2.7 Surface Resistance r_s

For the surface resistance r_s calculation the leaf area index (LAI) has to be estimated. As only one Sentinel-2 scene was available for each of the eleven days, only one LAI value could be calculated per day. Thus, the surface resistance is considered constant over the day. For r_l a constant value of 100 s m^{-1} , as suggested by the FAO in Allen et al. (1998, chapter 2), was used. In reality the stomatal resistance is crop dependent, but as not all crop types in the study area were known, a constant value for all fields seemed appropriate. This will of course also induce an error to the result. To calculate the LAI the method of (Delegido et al., 2013) was used (Eq. 2.15). The NDI was calculated using the Sentinel-2 bands 4 and 5 (Eq. 2.16).

$$r_s = \frac{r_l}{LAI_{active}} \quad (2.14)$$

r_s : Surface resistance [s m^{-1}]

r_l : Stomatal resistance of the well-illuminated leaf [s m^{-1}]

LAI_{active} : Leaf area index of the active part of the plant ($LAI \cdot 0.5$) [-]

$$LAI = -0.91876 + 13.448 \cdot NDI \quad (2.15)$$

LAI = Leaf area index [-]

NDI = Normalized differential index [-]

$$NDI = \frac{B4 - B5}{B4 + B5} \quad (2.16)$$

B4: Band 4 of Sentinel-2 (665 nm)
 B5: Band 5 of Sentinel-2 (705 nm)

2.6.2.8 Net Radiation R_n

An important factor for the net radiation calculation is the albedo. It is derived from the Sentinel-2 scene and assumed constant over the day. The irradiance measured with the FloX-Box was summed up over the whole spectrum for each time step and averaged for the hourly and daily calculations. The FloX-Box only collects data during daylight, hence there are no measurements during night-time. Due to this, a constant time of 6.00 – 22.00 UTC was used for all calculations. However, this can lead to too high ET values as some of the data may be cut of. Additionally, it also limits the hourly means calculation to daytime.

$$R_n = (1 - \alpha) \cdot E_{TOC} \quad (2.17)$$

R_n : Net radiation at crop surface [$\text{MJ m}^{-2} \text{ day}^{-1}$ or hour^{-1}]

α : Albedo [-]

E_{TOC} : Top of canopy irradiance [$\text{W m}^{-2} \text{ nm}^{-1}$]

The albedo is the integration of the at surface reflectance across the shortwave spectrum (D'Urso & Belmonte, 2006). It can be calculated as follows:

$$\alpha = \sum | \rho_{bi} \cdot \omega_{bi} | \quad (2.18)$$

α : Albedo [-]

ρ : Surface reflectance

ω : Weighing coefficient

bi : Band of Sentinel-2

To have the same spectral range as the FloX-Box irradiance measurements, only the Sentinel-2 bands 2 – 8 were used for the albedo calculation. The same weighing coefficients ω_{bi} for the Sentinel-2 bands as in Vanino et al. (2018) were used and can be found in Table 2.1.

2.6.2.9 Ground Heat Flux G

According to the FAO and Calanca et al. (2011) the ground heat flux is 10% of the net radiation.

$$G = 0.1 \cdot R_n \quad (2.19)$$

G : Ground heat flux [$\text{MJ m}^{-2} \text{ day}^{-1}$ or hour^{-1}]

R_n : Net radiation at crop surface [$\text{MJ m}^{-2} \text{ day}^{-1}$ or hour^{-1}]

2.7 Gross Primary Production

Gross Primary Production (GPP) describes the carbon flux from carbon dioxide to carbon compounds in plants by using photosynthesis on an ecosystem level (Bandaru et al., 2013; Beer et al., 2009). For the thesis a light use efficiency (LUE) based approach (Eq. 2.20), which uses climate and satellite data, was used (Monteith, 1972, 1977).

$$GPP = PAR \cdot fAPAR \cdot LUE \quad (2.20)$$

GPP: Gross primary production [$\text{g C m}^{-2} \text{ day}^{-1}$]

PAR: Photosynthetically active radiation [W m^{-2}]

fAPAR: Fraction of absorbed PAR [-]

LUE: Light use efficiency [$\text{g C m}^{-2} / \text{MJ APAR}$]

2.7.1 Photosynthetically Active Radiation

The photosynthetically active radiation (PAR) is the part of the spectrum which plants can use for photosynthesis. This part lies in the visual part of the spectrum (400 – 700 nm) of the terrestrial sunlight (Figure 2.4) (González & Calbó, 2002). According to multiple sources PAR is about 45% of the global radiation (González & Calbó, 2002; Xin et al., 2015). Therefore, this percentage of the global radiation measurements from the Wynau meteo station was used to estimate PAR.

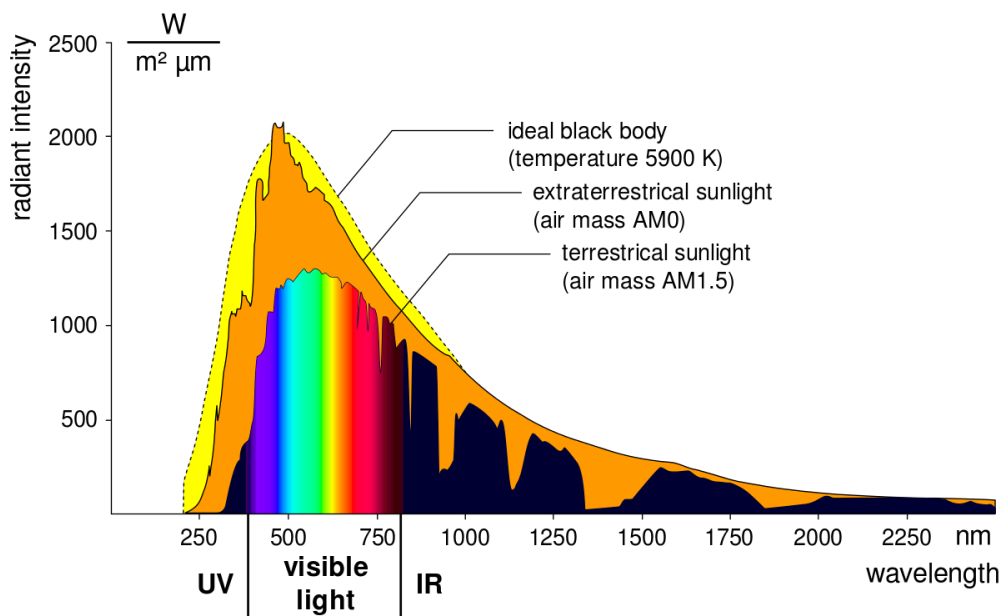


FIGURE 2.4: Spectrum of the solar radiation on Earth, in the extraterrestrial and terrestrial situation. The photosynthetically active radiation represents the visible wavelength area of the total global radiation spectrum (terrestrial situation) (Degreen & Locusta, 2020).

2.7.2 Fraction of absorbed PAR

A relation between the fraction of absorbed PAR (fAPAR) and the Enhanced Vegetation Index (EVI) has been detected (Lin et al., 2019). This index is more sensitive to canopy structural variation than to chlorophyll content, which is for instance detected by the NDVI (Glenn et al., 2007). It is also able to better explain the seasonal dynamics and inter annual changes of the carbon exchange (Xiao et al., 2005). This way the vegetation signal is optimised by a de-coupling of the canopy background signal (Huete et al., 2002). The index is calculated as follows:

$$EVI = G \cdot \frac{\rho_{NIR} - \rho_{RED}}{\rho_{NIR} + C_1 \cdot \rho_{RED} - C_2 \cdot \rho_{BLUE} + L} \quad (2.21)$$

EVI: Enhanced vegetation index [-]

ρ : Surface reflectance

L: Canopy background adjustments

C_1, C_2 : Coefficients of the aerosol resistance term

G: Gain factor

The coefficient values proposed by Huete et al. (2002) $L = 1$, $C_1 = 6$, $C_2 = 7.5$ and $G = 2.5$ were used. For NIR the Sentinel-2 band 8, for RED band 4 and blue band 2 were used. fAPAR was assumed constant over the course of a day.

2.7.3 Light Use Efficiency

The LUE describes how efficient the photosynthesis of the studied biome or plant is and converts the incoming radiation to stored carbon (Wei et al., 2017). It accounts for different conditions from the environment which can have an effect on the photosynthesis of the plants (Wolanin et al., 2019). LUE depends on the type of plant, but as not all plants in the study area are known, the global average value estimated by Wei et al. (2017) of $1.23 \text{ g C m}^{-2} / \text{MJ APAR}$ was used as a constant value for all days of the study period.

2.8 Water Use Efficiency

There are different approaches to calculate Water Use Efficiency (WUE). For this thesis the GPP based approach was used, which is defined as the ratio between the carbon gain, expressed through GPP, and water loss due to evapotranspiration (Tian et al., 2010). This is also named as biomass based WUE as it depends on the new biomass produced through photosynthesis (Qiu et al., 2008). WUE was calculated as hourly and daily means using (Eq. 2.22).

$$WUE = \frac{GPP}{ET} \quad (2.22)$$

WUE: Water use efficiency [g C/kg H₂O]

GPP: Gross primary production [g C/m² day]

ET: Evapotranspiration [mm H₂O/day]

2.9 Performance Indicators

Performance indicators (PI) were developed to help farmers understand and interpret the results of the calculated parameters. They should add value to abstract scientific data, so that all users can use the results and not only remote sensing scientists. To test the indicators, the same data was displayed in a normal scientific way and in a more illustrated, visualised way. This was achieved using the R package Shiny which enables the generation of interactive user interface for the data.

2.9.1 Yield

The possible increase or decrease in yield of a field was estimated by using the GPP parameter. The summed differences between the chosen field and the chosen crop type for all images were calculated. Depending on the resulting value, it is either a possible yield increase (positive value as the field has higher a GPP sum as the class) or yield decrease (negative value).

2.9.2 Water

In a similar way as the yield PI, the water PI calculates a possible water loss or water saving by using the ET parameter. If the field has higher summed ET values as the chosen crop type, more water is unnecessarily used in the production of the crops and, therefore, water is lost. This PI is only usable when the same crop in the same time frame is used for the comparison.

2.9.3 Productivity

As a third PI, the productivity of the selected fields was compared to the possible productivity for the crop type found in literature. As reference values the data from (Swiss Granum, 2017) for winter wheat, summer wheat and maize was used. As the productivity is the yield per area the additional input of the field area is necessary for this calculation.

3 Results

Evapotranspiration (ET) was calculated using the Penman-Monteith (P-M) equation (Eq. 2.3) and the gross primary production (GPP) with the light use efficiency approach. From these two parameters the water use efficiency (WUE) was deduced. This was done for both daily and hourly means. Using a multi-temporal data stack of three indices (LAI, GLI, CVI) the fields in the study area were classified into three different crop types. Using these classes and the three parameters, performance indicators (PI) were developed and implemented in an R Shiny app.

3.1 Classification of the Study Area into Crop Types

The result of the classification (Figure 3.1) shows test field 3 in class 1 (blue), fields 4 – 6 in class 2 (yellow) and fields 1 – 2 in class 3 (red). To define the kind of crops in each class was very difficult to accomplish. The class images were compared to the three available APEX images of the area and the Sentinel-2 images to determine the planting and harvesting periods of the different field classes. Together with the seeding and harvesting times stated on landwirtschaft.ch (2020) the crops within the three different classes were identified. Type 1 fields are still brown/bare in June and dark green from July on. Hence, these fields have summer crops planted. Type 2 fields are green in all of the images used for the classification. Therefore, these fields represent a mixture of maize and other crops. The last type shows brown/bare fields in the images of July and September. This is the harvesting time of winter crops. Test field 4 belongs to this class, which is the only field the crop type is known. According to the research site description, winter wheat was planted in the 2018/19 season, which falls into the winter crop category. There are fields in all three classes which could be grass or cut-down crops.

3.2 Calculation of the Base Maps

3.2.1 Leaf Area Index Values

The first parameter to calculate was the LAI which was then used as input for the ET calculation (see section 2.6.2.7). Eliminating pixels with LAI values lower than or equal to 0, enabled the filtering out of streets, buildings and water still present in the study area. Only the remaining pixels were used to calculate the ET in the next step. Over the time span of the eleven analysed dates the LAI had a total range of 0 – 6.3. The mean daily values for the whole study area and the three classes can be found in Figure 3.2. More detailed values for each of the six test fields can be found in Table A.1.

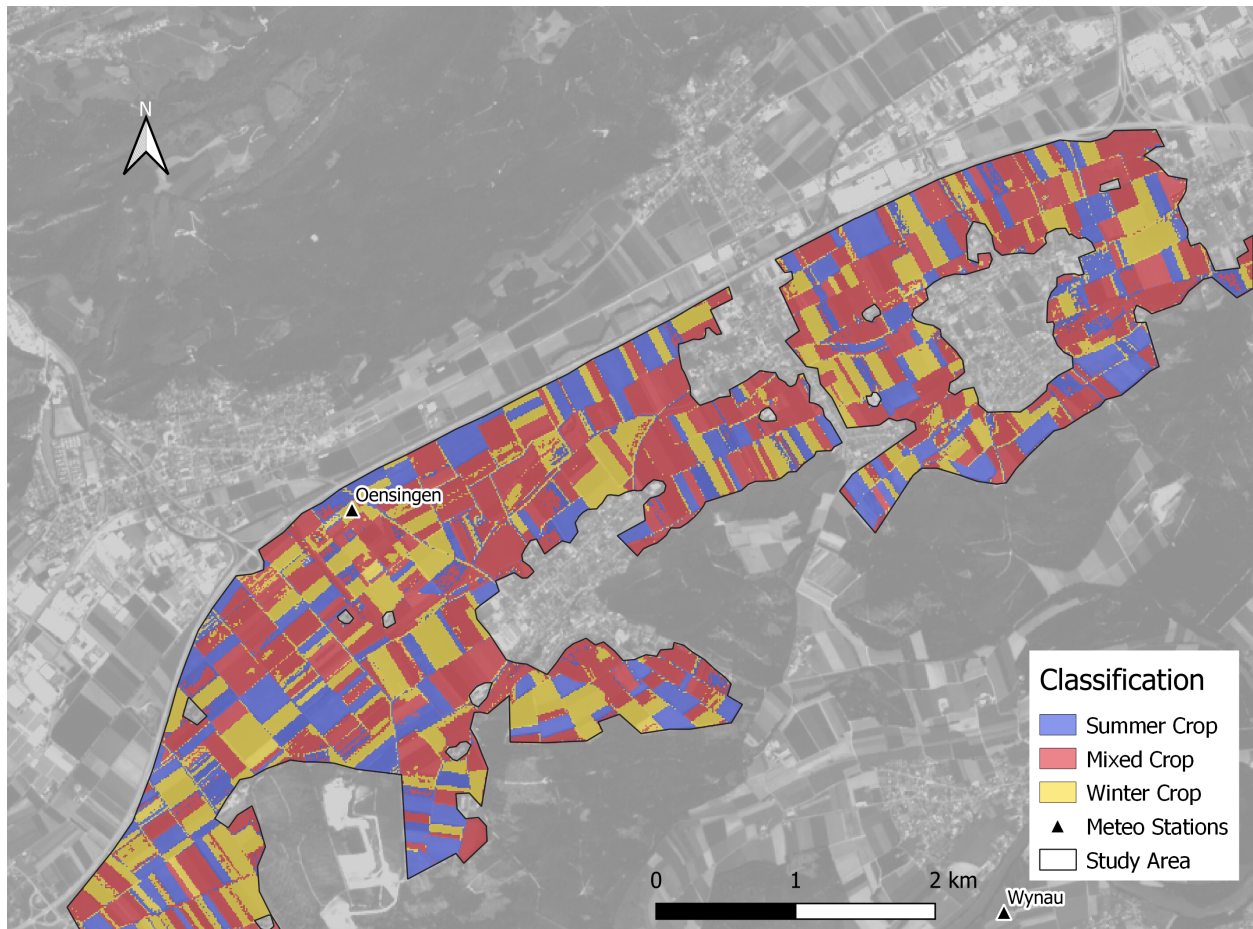


FIGURE 3.1: Classification map of the three crop types (summer, winter and mixed crop) found in the study area. The supervised classification was achieved by using a multi-temporal layer stack of three indices (leaf area index, green leaf index, chlorophyll vegetation index) and the spectral angle mapper as classifier. The Sentinel-2 scene of June 19th 2019 was used as background.

Figure 3.2a represents the changes of the daily mean values of LAI during the study time span, with lower values in the summer months and higher values in both spring and autumn. This distribution is also visible in both the winter crop and mixed crop classes, but not in the summer crop class which shows a different trend (Figure 3.2b). Figure 3.3 shows the distribution of the daily mean LAI values over the study area displayed as a heat map on 19th of June 2019. Darker colours indicate higher LAI values and represent mostly fields of the winter and mixed crop class. As the LAI is based on the Sentinel-2 image, there is only one value available per day. Therefore, it is assumed constant over the day for further calculations and no hourly results are available.

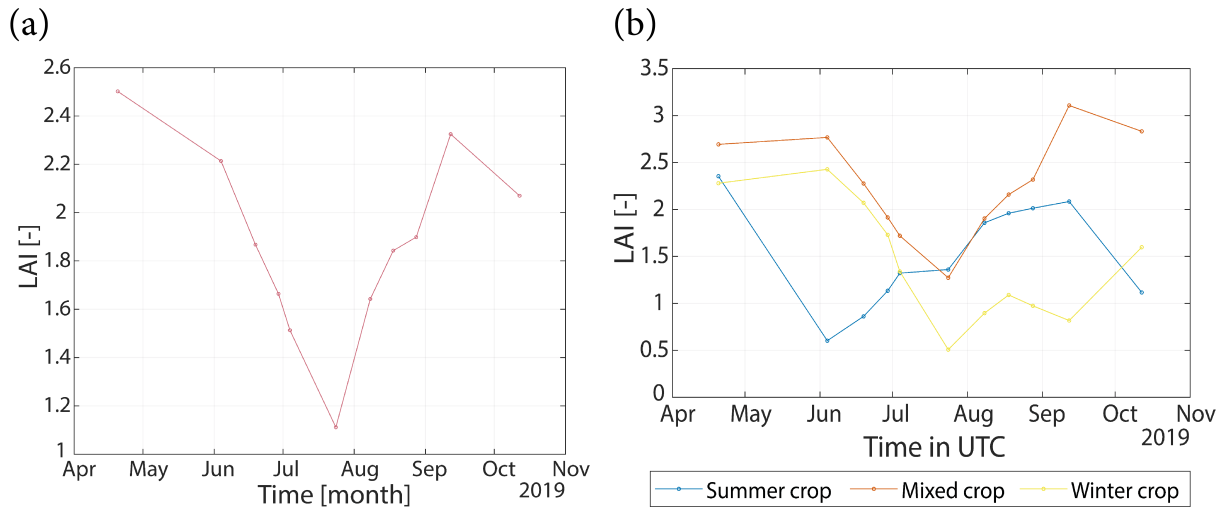


FIGURE 3.2: (a) Calculated daily mean leaf area index values for the whole study area and (b) the three crop type classes over the year 2019 using the method of Delegido et al. (2013).

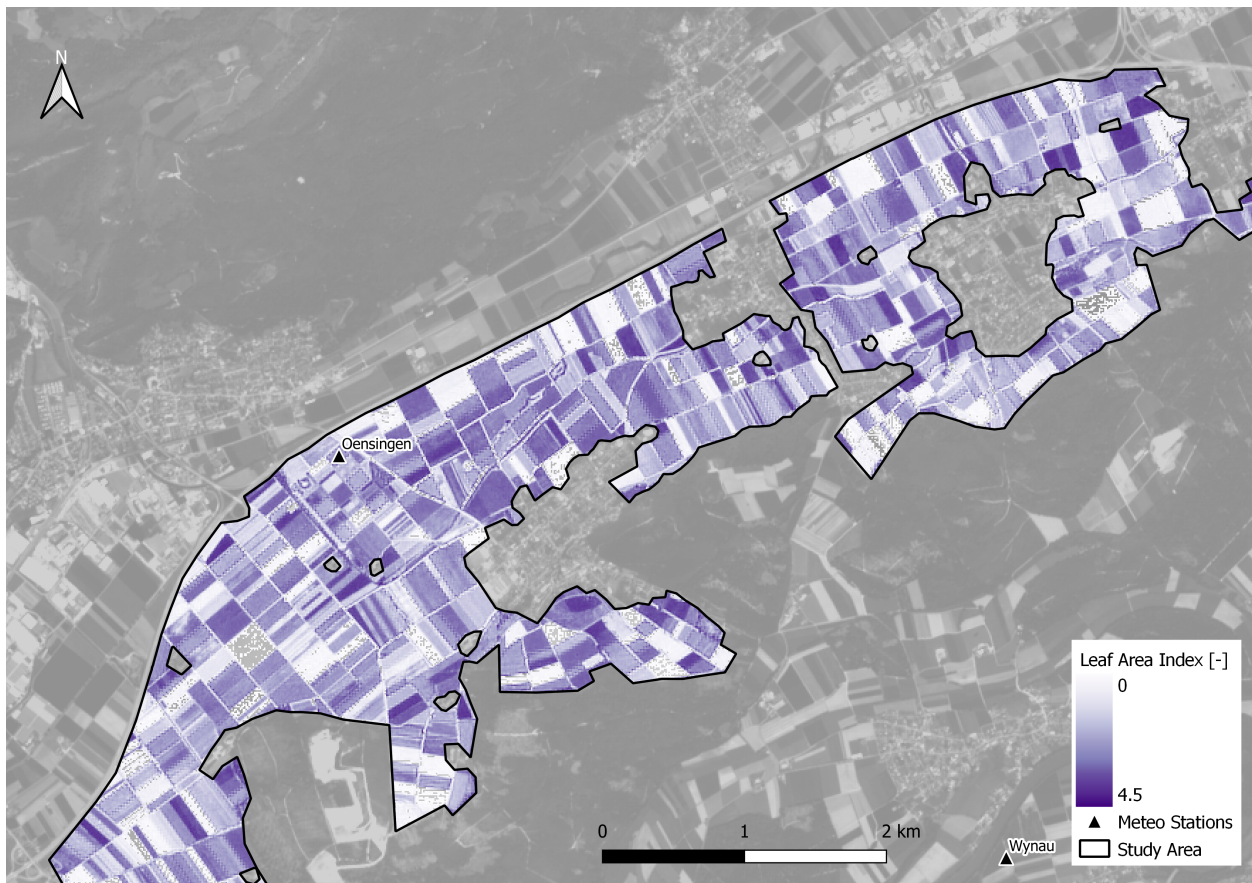


FIGURE 3.3: Heat map of daily mean leaf area index values of 19th June 2019 for the whole study area with darker colours indicating a higher leaf area index. The Sentinel-2 scene of June 19th 2019 was used as background.

3.2.2 Evapotranspiration Values

In a second step, the remaining pixels after filtering with the LAI were used to calculate ET with the aid of the Penman-Monteith equation for both hourly and daily time steps. Figure 3.4 shows the hourly variation of the measured days in 2019. The results range from 0 – 0.6 mm/hour with the highest values occurring during midday. It can also be seen that the amount of water evapotranspirated at the midday peak varies over the year, with highest values in the hot summer months. Early in the morning and in the evening even higher and lower values can occur (not displayed in the graph). The FloX-Box’s recording time is the same over the whole period but sunrise and sunset are changing. Due to this, the measurements are not always meaningful as they only work during sunshine. Hence, only data from 6.00 – 22.00 UTC are presented in the graphs.

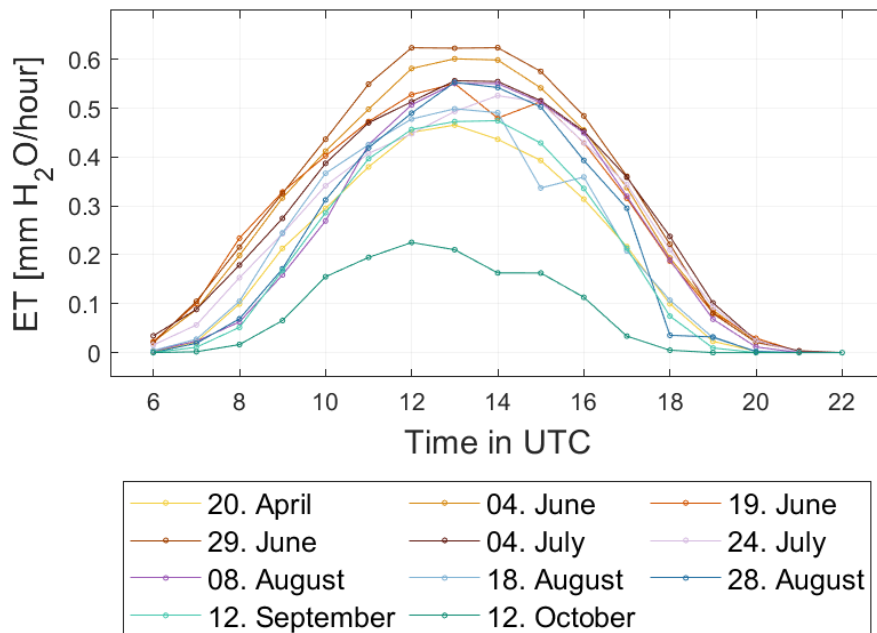


FIGURE 3.4: Calculated mean hourly evapotranspiration for the whole study area for all eleven days in the study period in 2019 using the Penman-Monteith equation.

The daily ET was calculated by summing up the hourly values. The total range of the daily ET over the eleven analysed days was 0 – 7.5 mm/day. In Figure 3.5 the mean values of the whole study area (a) and the three field classes (b) can be seen. This figure enables the higher ET values in the summer months to be seen, and lower values in spring and autumn. It shows an opposite course over the year than the LAI values (Figure 3.2a). More detailed values can be found in the appendix (Table A.2). To visualize the computed ET data, a heat map of the study area for June 19th 2019 was created (Figure 3.6). The lightest blue values indicating low ET, belong mostly to the summer crop class. When comparing to Figure 3.5b it can also be seen that this class has the lowest values on June 19th. The other two crop classes are very similar on this date and have, therefore, similar dark colours in the heat map.

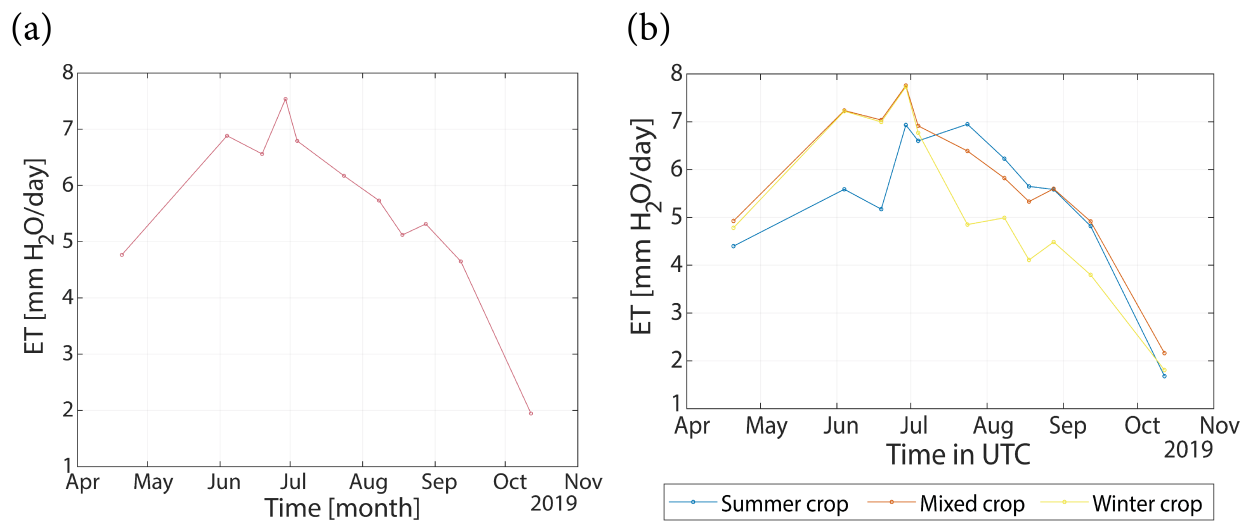


FIGURE 3.5: (a) Calculated mean evapotranspiration for the whole study area and (b) the three crop type classes over the year 2019 using the Penman-Monteith equation.

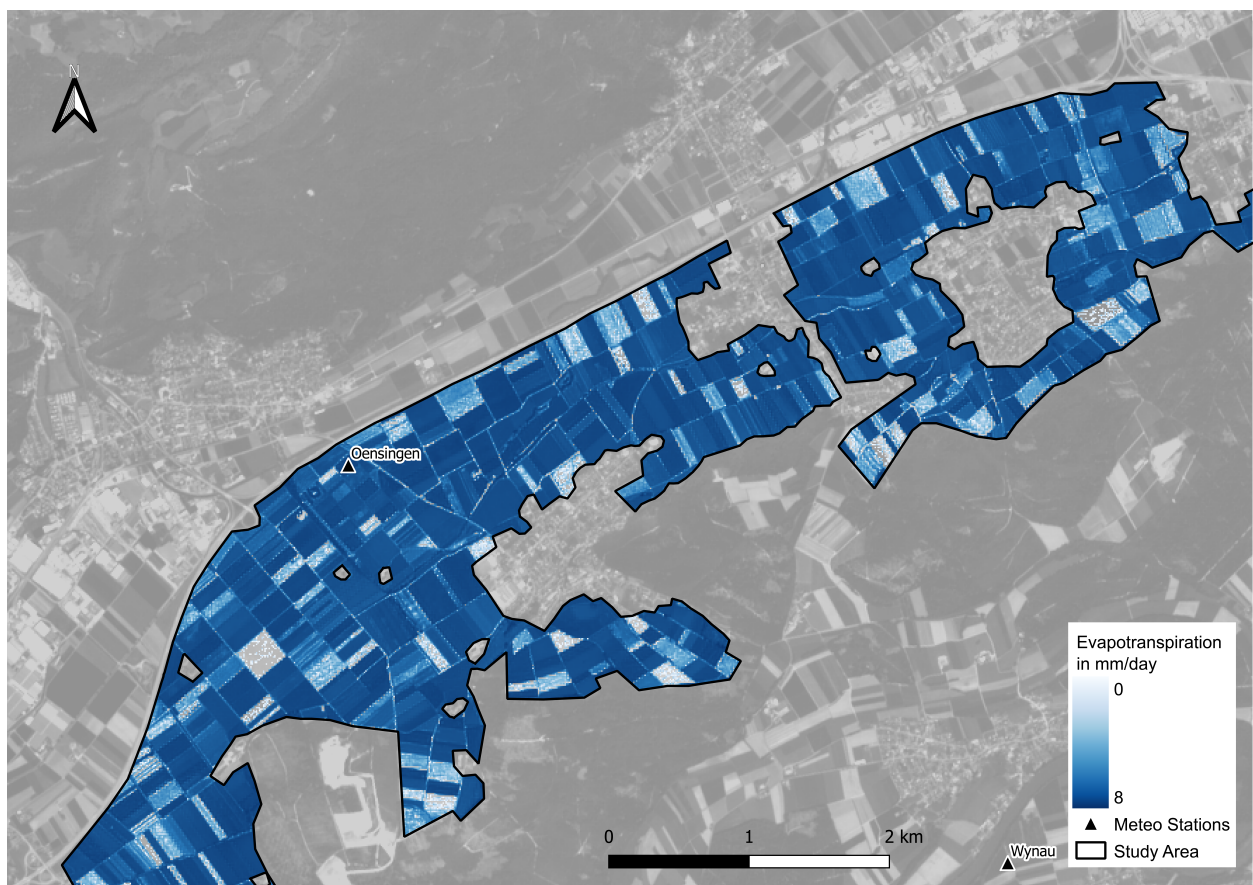


FIGURE 3.6: Heat map of daily mean evapotranspiration of 19th June 2019 for the whole study area. The darker blue colour indicates higher evapotranspiration. The Sentinel-2 scene of June 19th 2019 was used as background.

As the study site in Oensingen has its own eddy flux tower, in situ measured ET is available for the same time period as calculated in this thesis. A comparison of the in situ measured ET (gap filled), the mean ET calculated over the whole study area and test field 4 can be found in Figure 3.7a. Test fields is represented in the graph as the flux tower is situated at that location. The match up data points of the in situ data and the modelled data for field 4 are also displayed in a scatter plot (Figure 3.7b). The trend line in grey is calculated using the least-squares approach and the blue line stands for the 1:1 dependency of the variables.

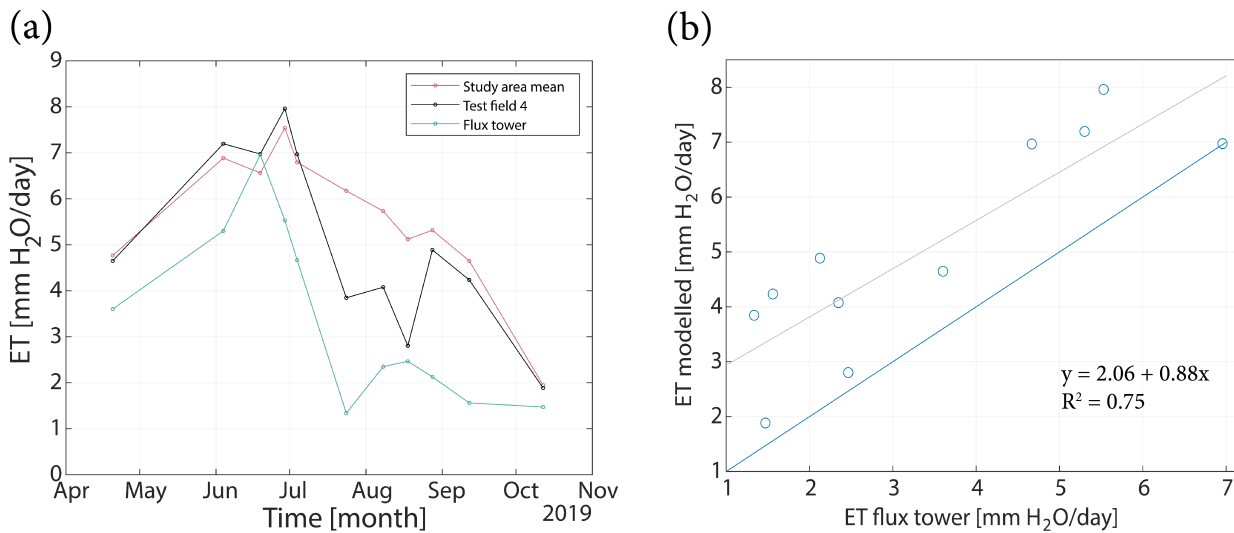


FIGURE 3.7: (a) Comparison of the in situ measured evapotranspiration at the flux tower in Oensingen which is situated in test field 4 with the modelled data for this field and the whole study area as line plot. (b) The direct comparison of field 4 data, modelled and measured, displayed as scatter plot with the 1:1 line in blue and the trend line ($y = 2.06 + 0.89x$, $R^2 = 0.75$) in grey.

3.2.3 Gross Primary Production Values

Using the light use efficiency approach, the hourly GPP values for the eleven available days were calculated. Figure 3.8 shows hourly variation of all of the eleven test days. The values range from 0 – 1.1 g C/m² hour with highest values in spring and early summer (yellow to orange colours). The shape of the daily course of the GPP values looks very similar to the ET on the same day (Figure 3.4) with the highest values around midday and the same downward peak at around 14.00 UTC. The daily values were calculated by summing the results of the hourly data. The calculations resulted in a total range of 0 – 36 g C/m² day. Figure 3.9a shows the results of all the mean values over the course of the study time span. There is a clear decreasing trend of GPP over time with some flatter parts with not much change during mid July to mid September. The mixed and winter crop classes a similar trend with the summer crop class having an opposite course (Figure 3.9b). More detailed values can be found in the appendix in Table A.3.

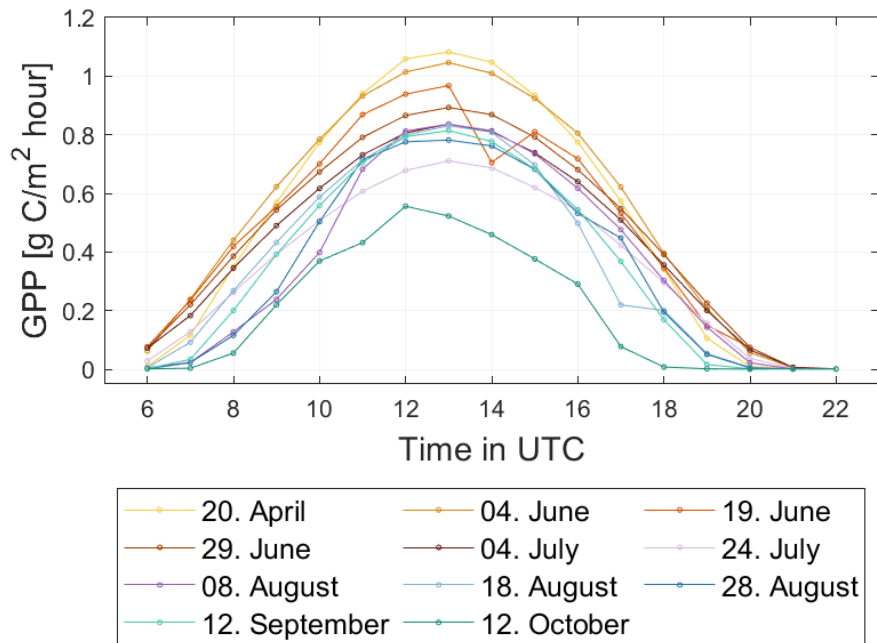


FIGURE 3.8: Calculated mean hourly gross primary production for the whole study area over the year 2019 using the light use efficiency approach.

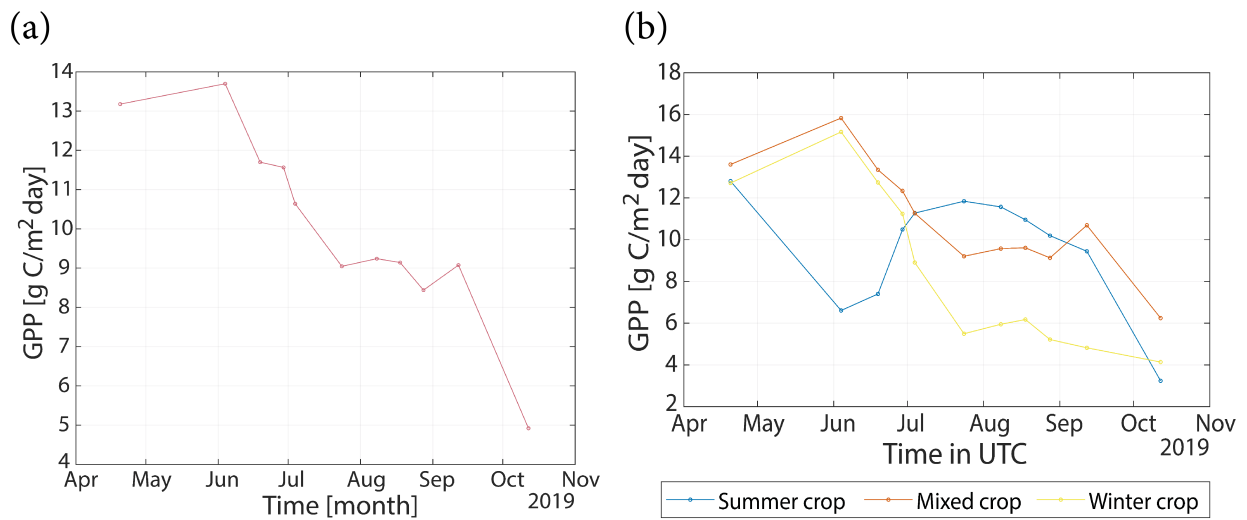


FIGURE 3.9: (a) Calculated daily mean gross primary production for the whole study area and (b) the three crop type classes over the year 2019 using the light use efficiency approach.

Similar to the LAI filtering, only pixels with GPP values equal or higher than 0 were used for further calculations. Figure 3.10 shows the distribution of the mean GPP values over the whole study area on the 19th of June for better visualisation of the spatial distribution of the values. At the time of the snap shot the winter crop is the class with the lowest values. This is reflected by the lightest coloured fields in the map. The fields with the highest GPP belong to the mixed crop class. The flux tower in Oensingen does not only measure ET but also estimates GPP using the nighttime partitioning method (Reichstein et al., 2005). With this information, the second modelled parameter used to estimate WUE could be validated with in situ measurements (Figure 3.11a & b). The trend line in grey is calculated using the least-squares approach and the blue line represents the 1:1 dependency of the variables.



FIGURE 3.10: Heat map of mean gross primary production of 19th June 2019 for the whole study area with darker green colour indicating higher a gross primary production. The Sentinel-2 scene of June 19th 2019 was used as background.

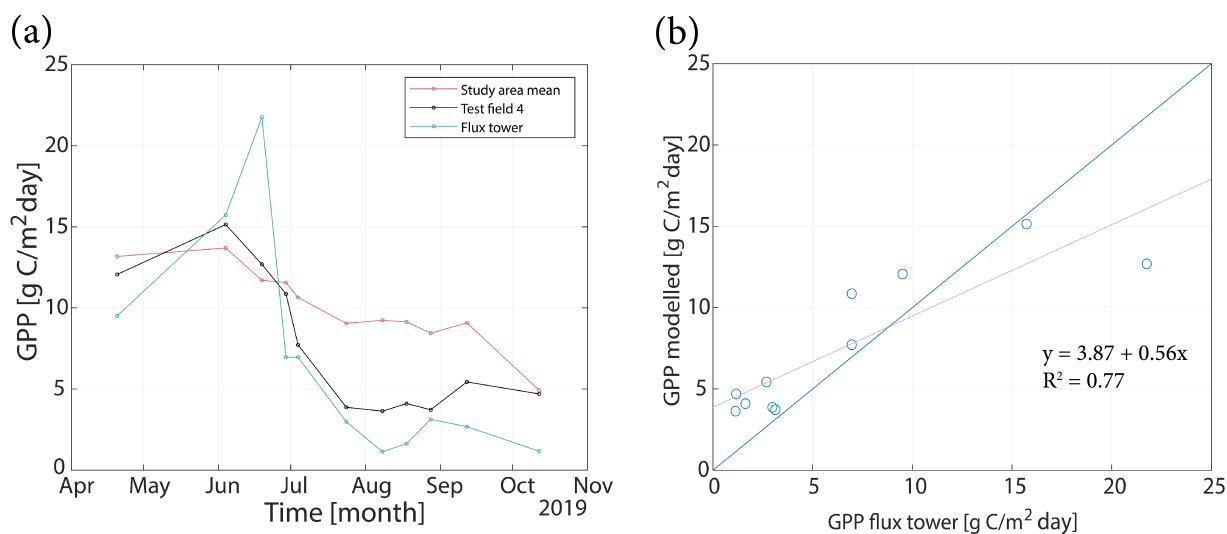


FIGURE 3.11: (a) Comparison of the in situ measured gross primary production at the flux tower in Oensingen which is situated in test field 4 with the modelled data for this field and the whole study area. (b) The direct comparison of field 4 data, modelled and measured, as scatter plot with the 1:1 line is in blue and the trend line ($y = 3.87 + 0.56x$, $R^2 = 0.77$) in grey.

3.2.4 Water Use Efficiency Values

Using the ET and GPP values for the WUE estimation a total range of areal mean of 0 – 8.9 g C/kg H₂O was calculated. When checking the absolute range of all values and not just the means, a very high maximum of over 100'000 g C/kg H₂O can be discovered. This however, is due to the calculation of the WUE (Eq. 2.22). If the ET value of a certain pixel is close to 0, the result for the WUE will be a very high number. For the same reason the standard deviation can be high for specific days and areas. For a better overview the mean values of the whole area (Figure 3.13a) and the three crop classes, (Figure 3.13b) should be used. All mean values and their standard deviation can be found in Table A.4 in the appendix. The hourly calculations of the WUE resulted in Figure 3.12a displaying the data for all days during the study time and Figure 3.12b for 19th of June 2019. Only the data between 7.00 – 18.00 UTC is used as the results before and after this time span have very high values. This is due to the same reason as described in Section 3.2.2. Within this daily time slot the results range between 1.2 – 5.7 g C/kg H₂O, with higher values in spring and autumn (yellow and blue-green colours). During this time period the variation within one day is also greater. 19th of June represents a more average distribution of values when compared to all the sampled days, however, when it is displayed separately, the inter daily variations can be seen. There are high values in the morning and evening, which are probably not usable measurements. But from around 9.00 – 14.00 UTC the graph shows a similar course as the ET and GPP results, with the highest values just before or around midday.

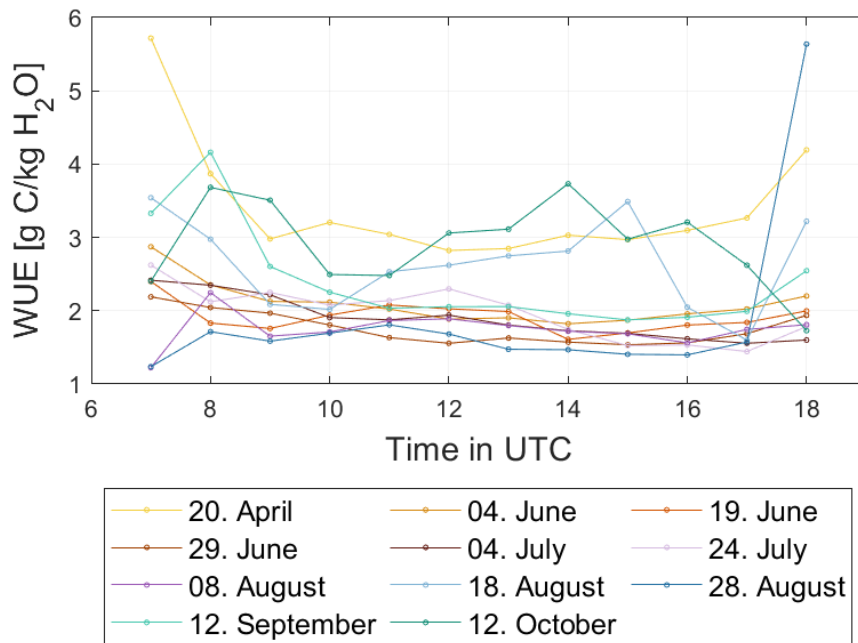


FIGURE 3.12: Calculated mean hourly water use efficiency for the whole study area over the year 2019 using the before estimated evapotranspiration and gross primary production.

For the daily mean WUE values the hourly data was summed up. Figure 3.13a shows the distribution of the daily mean values over the course of the study, with low values in summer (except for one peak in August) and higher values in spring and autumn. The daily mean of the three classes (Figure 3.13b) is the result of dividing the mean GPP by the mean ET of the respective classes. All classes also display a similar trend as the daily mean of the whole study area, and are relatively similar in value range. Figure 3.9b allows to pin point the outlier in August to the winter crop class displayed in yellow. A heat map describing the mean WUE values over the whole study area, calculated by pixel wise division of GPP/ET can be found in Figure 3.14. The lightest colour indicating low WUE can be found in fields of the winter crop class. Highest values are from summer crop and mixed crop fields.

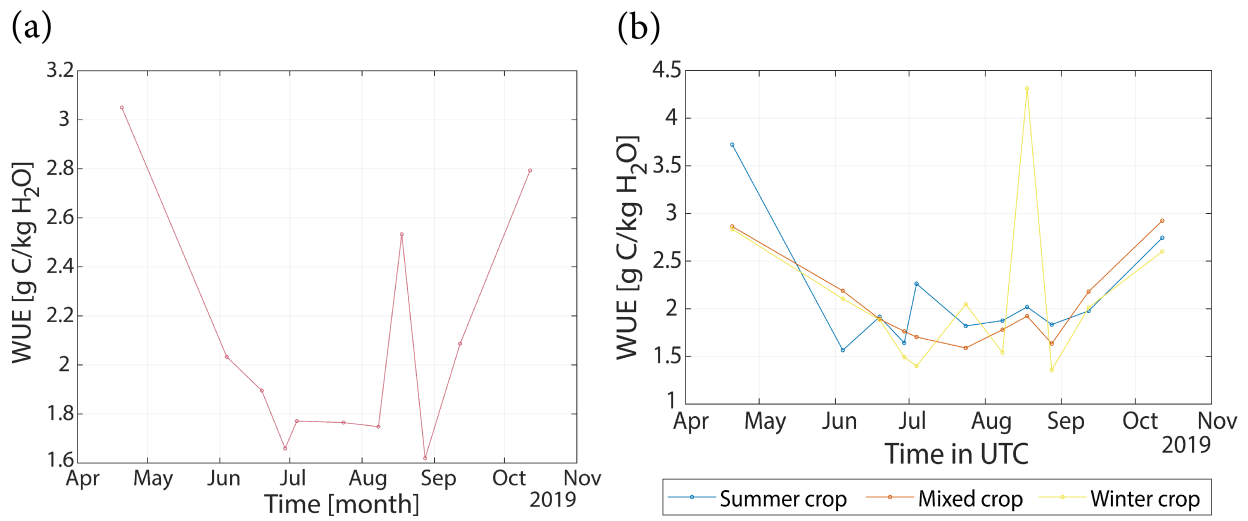


FIGURE 3.13: (a) Calculated daily mean water use efficiency for the whole study area and (b) the three crop type classes over the year 2019 using the before estimated evapotranspiration and gross primary production.

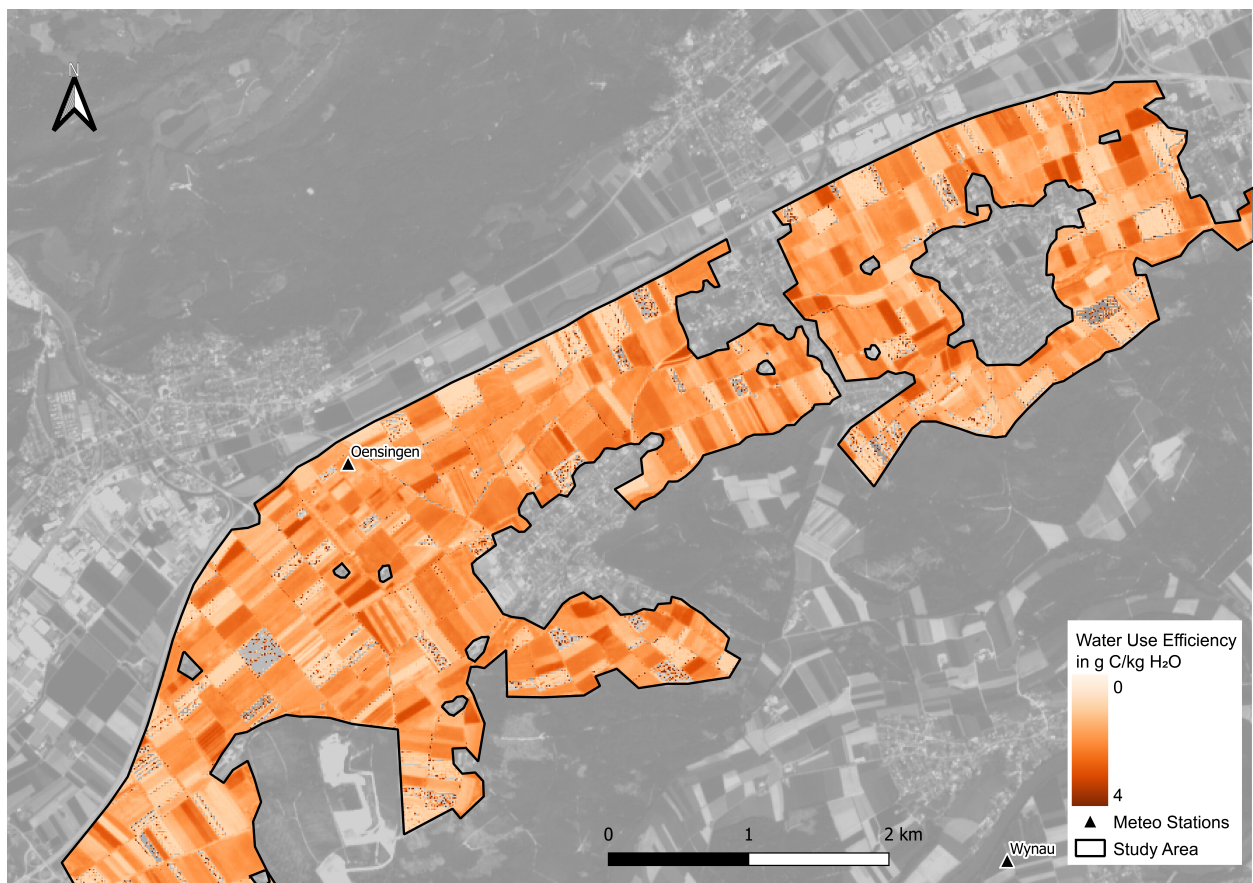


FIGURE 3.14: Heat map of daily mean water use efficiency of 19th June 2019 for the whole study area calculated by pixel wise division of evapotranspiration and gross primary production. Higher water use efficiency is displayed in darker orange colour. The Sentinel-2 scene of June 19th 2019 was used as background.

3.3 Performance Indicators

An app was created with the aid of the R Shiny package (RStudio, 2020) to interactively display the calculated results. On its start page, information is given about the research conducted for this thesis (Figure 3.15). The two tabs "Daily Data" and "Performance Indicators" enable an interactive exploration of the results of this study.

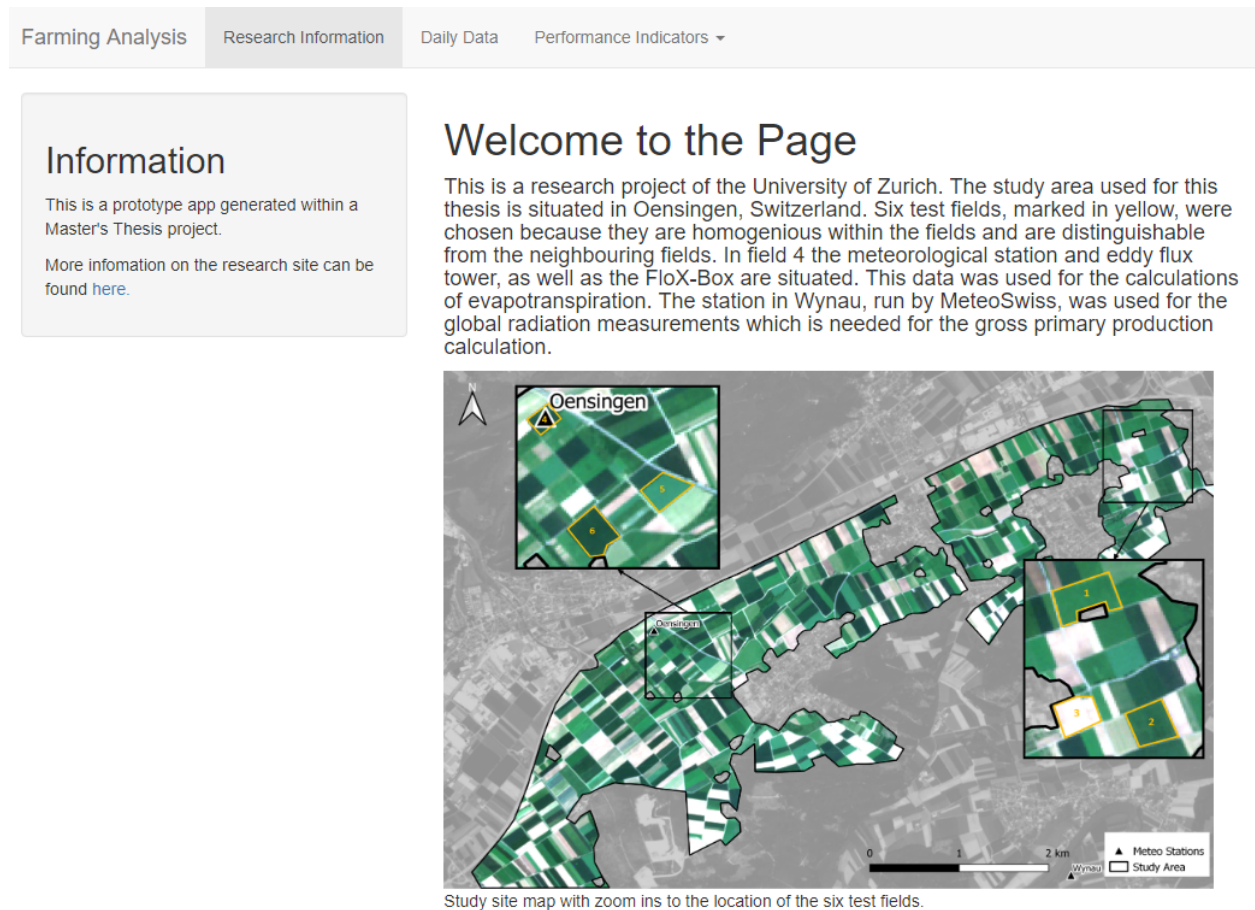


FIGURE 3.15: Start page of the R Shiny app with information about the research and a map of the study site with the six test fields marked.

Depending on the chosen test field, crop type and parameter (ET, GPP, WUE), the course of the daily values is displayed over the year 2019. With this, the own field can be compared to the mean value of the same crop type in the study area. As example Figure 3.16 illustrates the "Daily Data" tab with the comparison of daily mean GPP of field 3 and the corresponding summer crop class. The data is displayed both as line and bar plot.

Choose your settings

These is precalculated data and not actually doing something other than plotting your choices.

Please choose one of your saved fields.

Choose Your field

Field 3 ▾

Choose the crop type to compare your field with. Area stands for all fields in the study area.

Choose the crop type

Summer crop ▾

As parameters the evapotranspiration, gross primary production and water use efficiency can be chosen. All three parameters were calculated using MATLAB.

Choose the parameter

Gross Primary Production ▾

Daily values

This is a visualisation of the daily calculated values of the selected fields and crop classes. They were calculated in MATLAB.

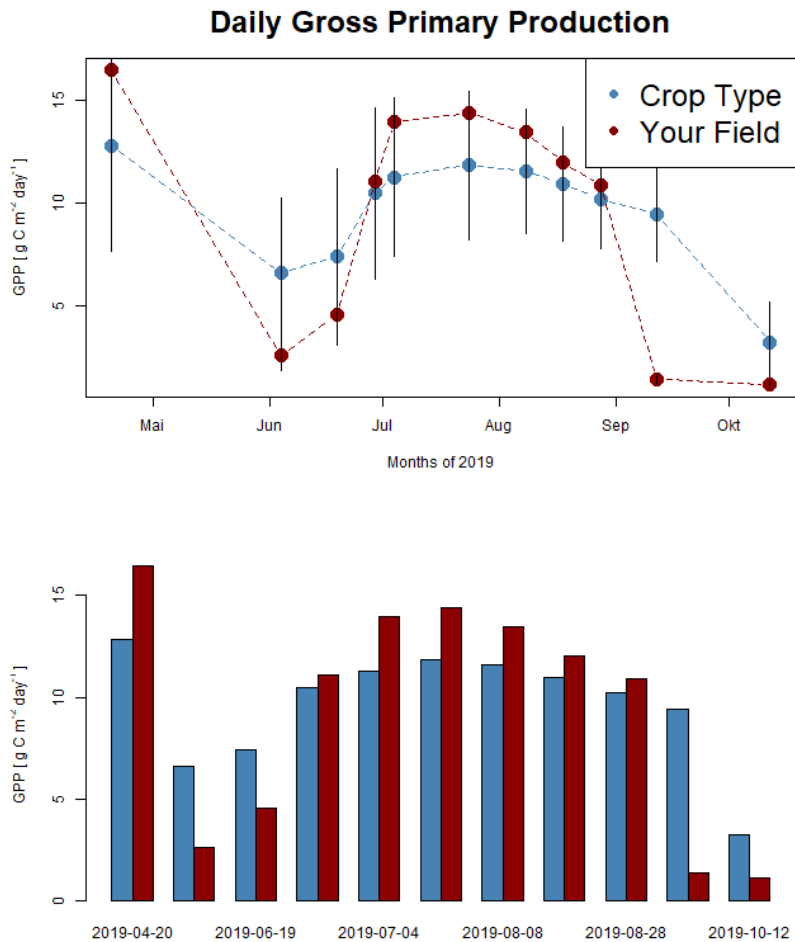


FIGURE 3.16: Daily mean gross primary production of field 3 (red) compared to the summer crops class (blue) in the app. The same data is visualised as line and bar plot. The black lines indicate the standard deviation of the means.

As a second step, three performance indicators, as described in Section 2.9, were implemented in the app. Using line and bar plots and adaptable graphics the PIs should help the user to understand the measured and calculated data. Additionally, the PI add value to the three calculated parameters by adding useful practical parameters such as yield, potential water loss and productivity. The three performance indicators are described in the following sections.

3.3.1 Yield

After calculating the yield differences between the selected test field and the crop type, the result was classified into three categories indicated with the position of the arrow in the adaptable graphics (Figure 3.17). The lowest category with a yield difference of < -10 , meaning the test field has a much lower yield as the average of the fields with the same crop type. This is represented with the red part of the speedometer. The orange intermediate category represents yield differences of $-10.1 - 10$, which is a mix of having lower and higher yield than the average. The highest class in the green area stands for yield differences > 10 . The unit used for the definition of the categories in 'GPP-values' in $\text{g C/m}^2 \text{ day}$. These values are transformed into % - numbers for more clarity and are accompanied with a statement whether a yield increase or decrease can be expected.

The same field and crop type class as in Figure 3.16 were selected to illustrate the possible yield outcome of 2019 in the app (Figure 3.18). The top plot describes the mean daily GPP of both the selected field (red) and crop class (blue). The bottom plot illustrates the absolute difference per measurement day as a bar. If the value is negative (less yield in the field than the overall class), the bar points downward and is coloured orange e.g. 12. September. As can be seen on the left side of the figure, the possible yield of field 3 is classified in the orange category. Additionally, the sentence below the graphic indicates a possible yield loss of 3.58% for the chosen field.

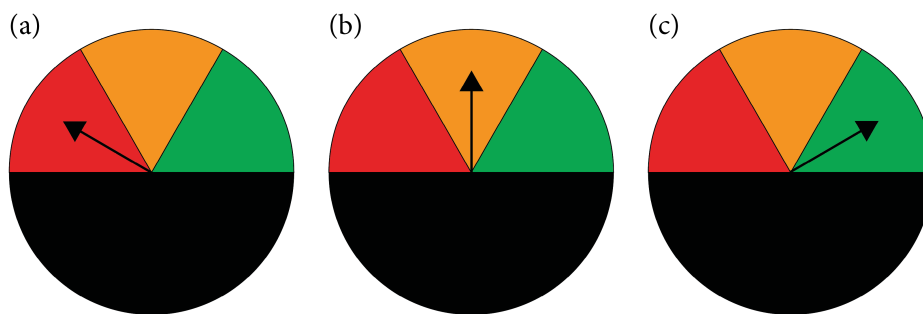


FIGURE 3.17: Depending on the yield difference between the chosen test field and crop type, one of the three categorised adaptable graphics appears in the app. They stand for (a) low, (b) middle and (c) high potential yield.

3.3.2 Water Use

Similar to the yield PI, the result of the difference of the water usage calculation was classified into three categories. Here, a water drop was chosen for the adaptable graphics with the different stages of fill for the three categories (Figure 3.19). The thresholds for the three classes are the same as described in Section 3.3.1 with the unit being the 'ET-values' in mm/day . As additional statement the potential water loss, if the difference between field and crop type is negative at the end of the year, or water saving, if the difference is positive, is given.

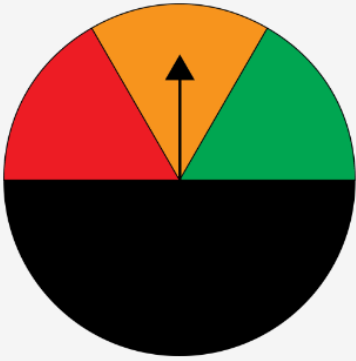
Choose your settings

Choose Your field
 Field 3 ▾

Choose the field that you want to analyse.

Choose the crop type
 Summer crop ▾

Choose the crop type to compare your field with. Area stands for all fields in the study area.



The absolute yield difference of your field to the chosen class is -3.78 GPP-units. This implies a possible yield decrease of 3.58 %.

Possible Yield Changes

Using the calculated GPP values of the chosen field, the possible yield increase or reduction compared to the fields with the same crop type can be estimated.

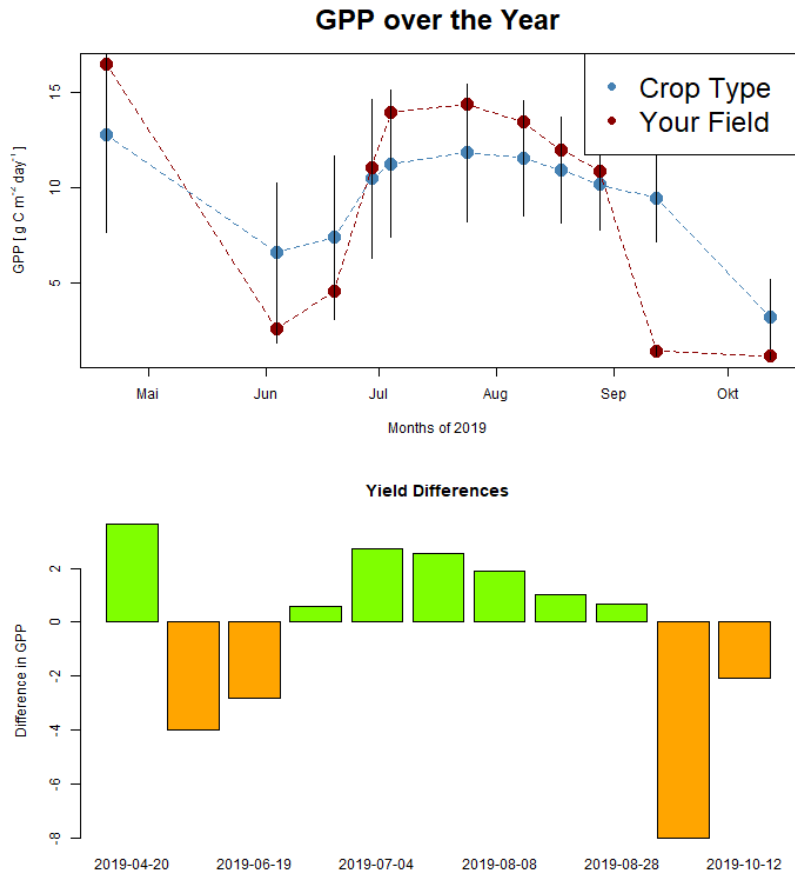


FIGURE 3.18: Possible yield of field 3 compared to the summer crop class in the app.

Using again the combination of field 3 and the summer crop class, the PI indicator for possible water losses and savings is illustrated in Figure 3.20. The top plot displays the distribution of ET of the field (red) and crop class (blue) over the year. The bottom plot indicates the differences in ET between the selected field and class. In contrast to the yield PI, having a negative water PI is a positive result, as it indicates less water use and therefore a water saving in this area. Due to this, negative bars are coloured in green and not orange as in the yield PI. The graphics indicates field 3 to be in the middle category and having a potential water saving of 6.66% over the year 2019.

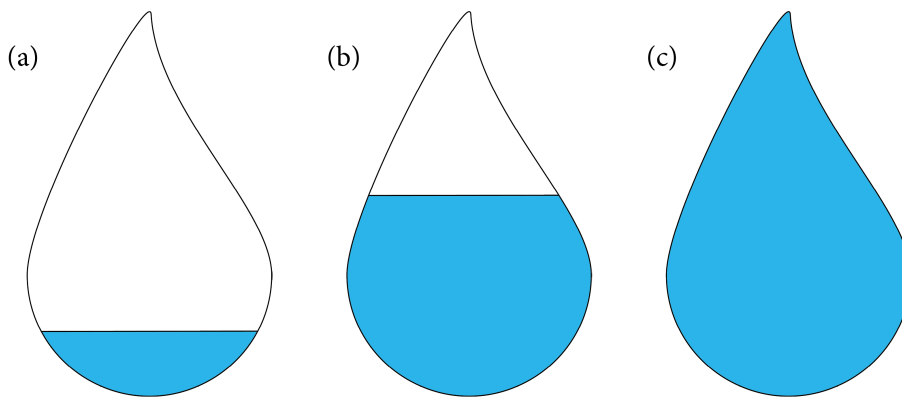


FIGURE 3.19: Depending on the potential water loss or saving of the chosen test field compared to the crop type, one of the three categorised adaptable graphics appears in the app. They stand for (a) low, (b) middle and (c) high water use.

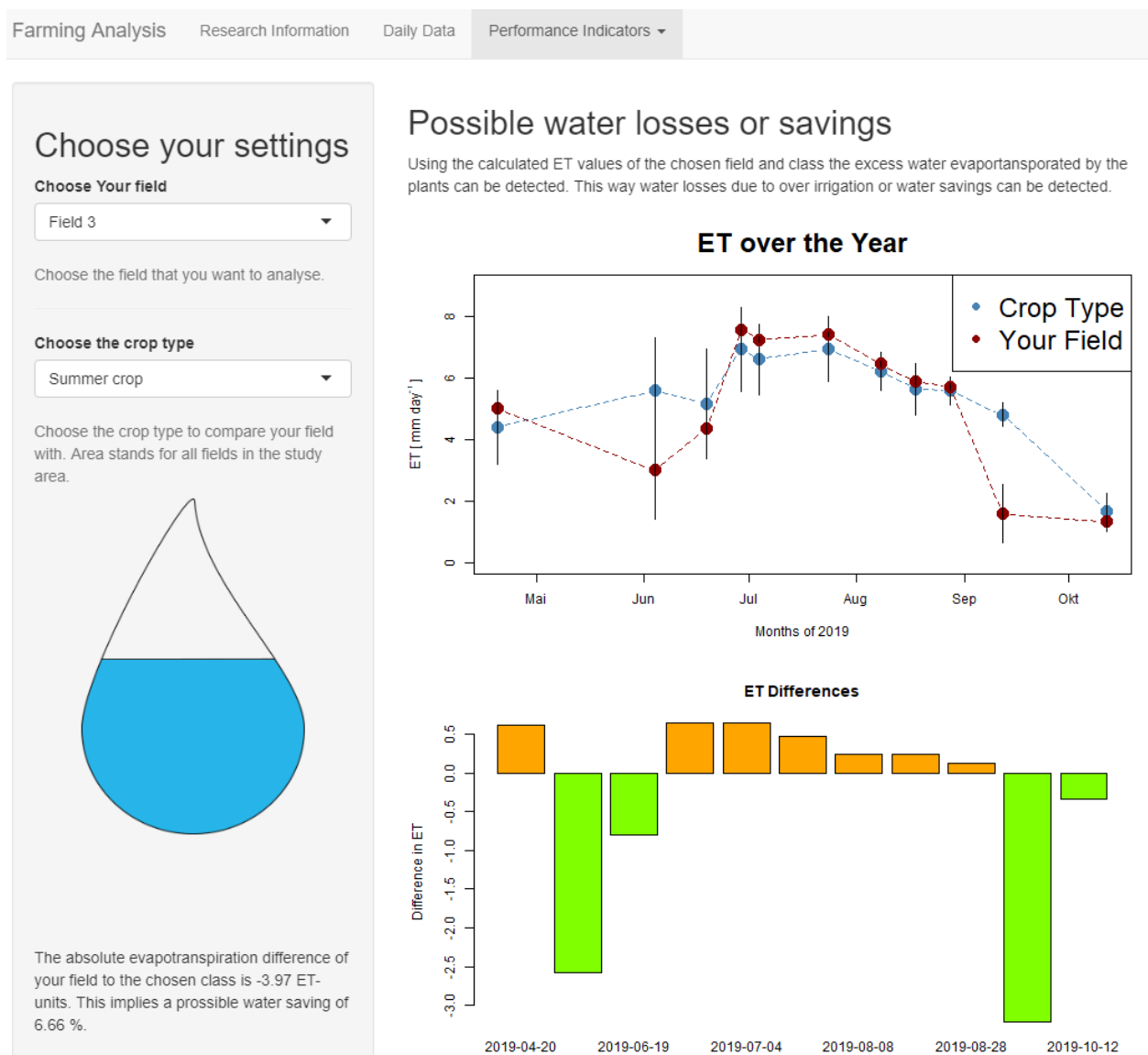


FIGURE 3.20: Water use of field 3 compared to the summer crop class in the app.

3.3.3 Productivity

As a third performance indicator the productivity of the selected test fields was analysed. Using a manual input of the field area in ha, calculated yields and literature reference values, the possible and actual productivity can be compared. As each of the three crop types contains multiple different crops, three representative crops were chosen to be used for the productivity calculation. For the summer crop, the productivity of 42.3 kg/Ar of summer wheat, for winter crop 58.4 kg/Ar of winter wheat and for the mixed crop type 108.9 kg/Ar of maize was used. After calculating, the app generates statements about the actual productivity of the selected yield and the productivity that could be possible on the same field in t/ha. The productivity PI is represented by a number of wheat stalks (Figure 3.21) depending on the percentage of productivity of the field compared to the possible productivity of the crop type. Less than 50% is the lowest category, between 50 and 75% is represented in the intermediate category and higher than 75% is the highest category with three wheat stalks.

The last PI of the productivity was also tested with field 3 (Figure 3.22). With an assumed field size of 50 ha the productivity of the field (red box) is not as high as literature references estimate (yellow box). Due to this the field is classified in the lowest category of the PI. The additional text below the graphic indicates the exact productivity value of 211.5 t/ha possible and 102.03 t/ha actual.

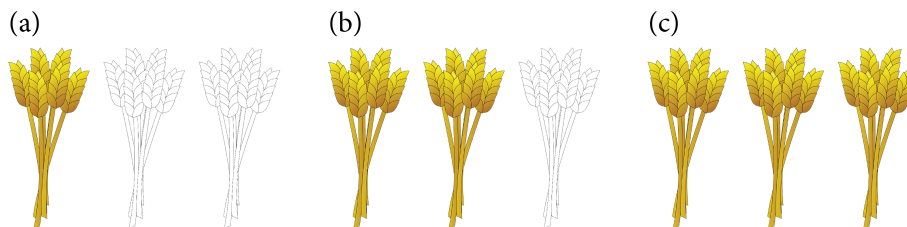


FIGURE 3.21: Depending on the productivity of the selected field compared to the possible productivity of the crop type class, one of the three categorised adaptable graphics appears in the app. They stand for (a) low, (b) middle and (c) high productivity.



FIGURE 3.22: Productivity of field 3 compared to the summer crop class in the app. An area of 50 ha was assumed for field 3.

For each of the six test fields the PI category was determined when they were compared to their respective crop classes (Table 3.1). For the productivity PI a field area of 50 ha was assumed for all six test fields.

TABLE 3.1: Category of the performance indicators of the six test fields when compared to their respective crop classes. Summer crop: field 3, mixed crop: fields 1, 2, winter crop: fields 4, 5, 6.

PI	Yield			Water Use			Productivity		
	High	Middle	Low	High	Middle	Low	High	Middle	Low
Field	1, 5	3, 6	2, 4	2	1, 3-6	-	-	-	1-6

4 Discussion

4.1 Interpretation of the Classification

Comparing one's own field with fields in which the same or similar crop types have been planted gives a more informative output for the end user, instead of only using the whole area as a comparison. For this, a classification of the fields in the study area was necessary. As the main focus of this thesis is not the classification of agricultural fields, a basic approach was used. The results of using this simple method is reflected in the low quality of the differentiation of the three crop classes. This effect is most obvious in the graphs which show the annual change of the three different classes (e.g. Figure 3.5b).

The shape of both the summer and winter crop class for the LAI (Figure 3.2b) and GPP (Figure 3.9b) parameters are reasonable, when compared to the sowing and harvesting times of the crops. Winter crops have the majority of their growing time over winter and spring, which accounts for the higher LAI and GPP values during the beginning of the study period ('landwirtschaft.ch', 2020). During this time the plants also consume and evaporate more water as they are more actively undergoing photosynthesis (Penning de Vries et al., 1989), which is reflected in the higher ET values (Figure 3.5b). After harvesting of the winter crop in June and July, all the described parameters drop to a constant lower value. The class of summer crop shows an contrary shape with lower values at the beginning of the year. This is consistent with the sowing time of around March to April. Values increase during peak growing season. After harvesting time in August the values should decrease as they do in the winter crop class ('landwirtschaft.ch', 2020). The results, however, show only a slight decrease and a drop in late September and October. This later harvesting time indicates the presence of another crop in this class, for instance maize which is harvested during this period of the year.

First, the third crop type class was meant to be the corn class. As the sowing time for maize is in late spring, LAI and GPP values should be low at the beginning of the study period with an increase over the summer months ('landwirtschaft.ch', 2020). With the harvesting time in autumn this signal should be the only crop class with high values in this time of year. Even if the third class has the highest values in this period it shows a contradicting shape over time and should rather look similar to the summer crop curve. Additionally, the two classes for corn and winter crop have a very similar shape in GPP over the year, with the difference of the corn class having generally higher values. This indicates that the two classes are not separated well and that most likely the corn class is a mixture of different crops including corn and winter crops. Due to this, the corn class was renamed mixed crop class.

Based on this, the summer crop class is the most reliable and the mixed crop class the least reliable within the classification. As the classification is only used as a means of comparison and visualisation of fields, the result is sufficient. Many other scientists are currently working on more sophisticated ways to classify agricultural fields e.g. Böhler et al. (2020) with promising results, which could be implemented in the future.

4.2 Reliability of the Base Maps

The resulting values and ranges of the four calculated parameters (LAI, ET, GPP, WUE) were compared to the in situ flux tower measurements conducted at the Oensingen site. Additionally, studies using the same model calculations were consulted to test the reliability of the base maps. This enables a validation of the two modelled input parameters ET and GPP for the WUE calculation, resulting in an indirect test for the reliability of the WUE.

4.2.1 Leaf Area Index Base Map

The LAI is an input parameter for the Penman-Monteith (P-M) equation and is, therefore a base for the ET calculation. Many studies have been conducted in Oensingen before and their results were used for validation of the here calculated data. In a study Laurent et al. (2013) estimated different biophysical and biochemical plant properties using APEX data at the Oensingen test site. They concluded that the LAI was the parameter with the highest similarity between model estimate and in situ measurement. The data measured in the study area has a range of 0 – 4.5, which is in the same region as the results of the mean daily LAI values calculated in this thesis.

The distribution of the calculated LAI values visualises the different growing and harvesting cycles of the agricultural fields (Figure 3.2a). Late April, with the beginning of this study most winter crops are already fully grown and no increase in LAI is visible when averaged over the whole area. With the harvest of the winter crops during spring and early summer and the sowing of summer crop and maize, a minimum LAI value is reached at the end of July. This is followed by a strong increase representing the growth of the before sown summer crops and maize plants and a decrease at the end of the study time span indicating the harvest of said crops. The curves for the different crop classes match up nicely with the sowing and harvesting times indicated on 'landwirtschaft.ch', 2020.

4.2.2 Evapotranspiration Base Map

As the result of the P-M equation, ET is one of the two modelled parameters in this thesis, which is then used to calculate the WUE.

Validating the modelled data with in situ data enabled the verification of the approach employed and to detection of possible error sources. Fortunately, the Oensingen site has its own flux tower from which the data was used. When comparing the modelled data to the in situ data from the flux tower (Figure 3.7a) a general overestimation of ET was detected. This was expected, however, as the P-M equation results in the potential evapotranspiration ET_0 and the flux tower

measurements represent the actual evapotranspiration (Cai et al., 2007). The modelled values and the flux data are similar in shape. High ET values at the beginning of the year, with the highest point in late June, describes the cycle of a winter crop, which field 4 had planted in this season ('Oensing site', 2020). The decrease beginning in July indicates the harvesting time of the field. Both features were modelled well by the P-M equation. The flux data remains relatively low for the rest of the year. The modelled values are much higher and even show an increase in late August. As the P-M equation is only applicable for vegetated areas with plants of a certain height, fields which lay bare or only have short grass growing, can lead to errors in the result due to low LAI (Farahani & Bausch, 1995). It is not certain that the pattern seen in Figure 3.7a is related to this. It was, however, observed that fields belonging to a crop class which was not within the crops' growing phase resulted in higher values than expected. The scatter plot also well illustrates the overestimation of the values computed by the used model, as all match up data points of field 4 and the flux tower are situated above the 1:1 line in blue (Figure 3.7b). The trend line in grey ($y = 2.06 + 0.88x$) is nearly parallel to the 1:1 line and has an R^2 of 0.75 which indicates a good correlation between measured and modelled data with a linear shift between actual and potential ET. The slight tilt of the line indicates a better estimation of higher ET values by the used model.

Comparing the calculated ET values of the whole area to different studies, the values calculated in this thesis are much higher. If the values are parted into the three different crop classes (Figure 3.5b) they are more similar to literature references. Paul-Limoges et al. (2020) found daily ET values of 1 – 4.5mm/day. This, however, was a study conducted in a forest area. A study from the US measured ET over crop land for four years and found a value range of around 0 – 4mm/day depending on the annual cycle (Tian et al., 2010). The daily peak of the ET values is reached on midday when the solar radiation has the highest impact (Chávez et al., 2008). On the distribution of ET over the single days (Figure 3.4a) the different length of days and the time when the sun is positioned at its highest in the sky can be determined. The peak in October is about one hour earlier than the ones during summertime and only have a third of the ET value. The curve is in general flatter, indicating that the plants are less active during this time of the year. Looking at the daily values of the three classes (Fig. 3.5b), the curves for both the summer and winter crop, show similar trends than the LAI (Figure 3.2b). As the plants are able to evapotranspire more water if the leaf area is bigger, and hence, more photosynthesis can be done by the plants, this dependency of parameters was expected (Penning de Vries et al., 1989). The mixed crop class shows highest ET values at the beginning of the summer with a decreasing trend over the year and with this looks very similar to a winter crop. In contrast to the winter crop class the ET is higher in the second half of the year. This again supports the description of a mixed crop class for the red curve.

The spatial distribution of ET in late June (Figure 3.6) visualises lower values in lighter colours. The lightest fields are all classified into the summer crop class. When compared to the RGB image of the area (Figure 2.1) most of these fields are light to dark brown, indicating that almost no plants have grown there, yet. The strong increase of growth is occurs at the beginning of July. The higher value fields are winter crops which have not been harvested and fields belonging to the mixed crop class. The ET measured there is probably from falsely classified winter crops, grass or some other crop type which is unknown.

From analysing and comparing the modelled data to the in situ flux tower measurements, it can be concluded that the ET data computed with the P-M equation can be used for this area. The equation is however very sensitive to non-vegetated ground and can therefore result in false values. Due to that, care must be taken when interpreting the results, as they also depend on the previously made classification.

4.2.3 Gross Primary Production Base Map

Using the light use efficiency (LUE) approach (Monteith, 1972, 1977), the GPP for the study area was modelled. As a second parameter to calculate the WUE, its reliability also had to be tested.

For the validation, the data from the flux tower in Oensingen was used (Figure 3.11a). Generally, the modelled data overestimates the GPP, only in the middle of June two data points of the flux tower have a higher value than the modelled ones. The comparison between the in situ data in yellow and the modelled values for field 4 in orange shows very similar shapes over the year. High values in spring when the winter crop, planted on the field, is growing and a decrease in June and July during harvesting. The rest of the year GPP values are low, as not much is growing on the field. Other than the modelled ET, the GPP is much more similar to the in situ data during this time. Only a small upwards peak in September is visible. The simulated GPP data points are much closer to the in situ measured data than the ET estimations. This is also reflected in the scatter plot. All points, except for the two in June, are slightly above the 1:1 line which indicated a small overestimation of GPP for the modelled data. The match up points are, however, scattered close to the 1:1 line, with the linear regression ($y = 3.87 + 0.56x$) having an R^2 of 0.77. This indicates a good estimation by the model. The trend line in grey crosses the 1:1 line at around $9\text{g C/m}^2\text{ day}$ which would mean that these model values are the most exact with the in situ data. However, the angle of the trend line is probably tilted this way to fit the two data points in June which could be outliers. If more data point were available, the trend line might be more parallel to the 1:1 line and describe a better fit between model and reality.

The speed of plant growth and with it the GPP is very different for every species. As there are probably multiple crops classified in the same crop type class, it is difficult to compare the GPP to reference values and even between the three classes. However, many sources estimate a daily GPP of $0 - 14\text{g C/m}^2\text{ day}$ (Paul-Limoges et al., 2018) and $0 - 20\text{g C/m}^2\text{ day}$ for a cropland site (Li et al., 2018; Revill et al., 2019), respectively. A similar value range was calculated in this study. The high values of $20\text{g C/m}^2\text{ day}$, was however only reached during peak growing season, if max values of field pixels were compared. If only daily mean values are taken into consideration, values as high as $17.8\text{g C/m}^2\text{ day}$ for test field 1 can be observed. The distribution of the hourly changes over the year (Figure 3.8a) look very similar to the ET values. As GPP is calculated by using the global radiation as proxy for PAR, this result was also expected. In the middle of the day and during the summer months more global radiation is present which can be used by plants to carry out photosynthesis and acquire more carbon (Penning de Vries et al., 1989). This increased activity is reflected in the growth of the plants which again is reflected in higher GPP. The mean daily values over the whole study area (Figure 3.9a) show a decreasing trend with a stagnant part in

summer. When compared to the curves of the three crop classes (Figure 3.9b) it shows a similarity to the mixed crop and summer crop classes, which are both also very similar to each other. This could mean that these two classes are more present in the study area and that the third class of summer crop, which looks different, has the smallest area. If the class has a smaller area the weight of the values in the mean calculation will be smaller. The only impact of this class is visible in the stagnant part in the curve in summer when the summer crops have higher GPP values than the winter crop class. There should, however, be a more prominent increase of GPP at the end of the year as maize has its peak growing season. Maize has been found to have the highest GPP values probably due to the height and volume of the plant and the greater photosynthetic capacity (Suyker et al., 2005; Xin et al., 2015).

The spatial distribution of the GPP values in mid June (Figure 3.10) looks similar to the ET distribution, with the lower value fields being the same. In contrast to the ET values, the distribution in the middle part of the data range is much more distinct. There are clearer differences between the fields, and fields next to each other can have very different values. For example there are fields with very high GPP values next to very low value fields in the north east corner of the study site. The same fields are not so different in the ET map. Consulting the classification map (Figure 3.1), it can be seen that the fields in this part belong to the mixed crop class. Fields in this class behave very differently for these two parameters being similar in ET and different in GPP. This could also render it difficult for the used classifier to distinguish between the fields in this class.

Comparing the in situ data to the GPP calculated using the LUE based approach leads to promising results. Having more data points could increase the validation significantly as the weight of the two outliers in June may be reduced. Even if LUE models show good results (Hu et al., 2013), there are multiple studies which model GPP using sun-induced fluorescence (SIF) instead of the EVI to estimate fAPAR (Damm et al., 2015; Paul-Limoges et al., 2018). As research goes on in this topic and the new ESA FLuorescence EXplorer (FLEX) mission is specialised for measuring vegetation fluorescence (Coppo et al., 2017), this approach is very promising for future use, as it enables the use of a direct signal instead of a simple band math index.

4.2.4 Water Use Efficiency Base Map

After testing the reliability of both ET and GPP, the result of the WUE calculation was indirectly tested as well. There could however be errors which are not related to the input parameters but to the calculation method or the previously made classification.

The WUE results were not validated with in situ measurements but compared to values from scientific papers. The range of WUE values found in literature is quite wide. Tian et al. (2010) calculated the WUE of different landcover types such as grassland, cropland and forest. For cropland they estimated a value of 0.54g C/kg H₂O, slightly less than the range of 0.68 – 0.89g C/kg H₂O calculated by Karam et al. (2007). For grapevines a WUE of 3 – 6g C/kg H₂O was calculated (Flexas et al., 2010). With values between 1.5 – 3 or even over 4g C/kg H₂O of the winter crop class the modelled WUE in this thesis is the high end of the literature value range.

The water use efficiency is the total water consumed by the plant during the growing season. This is the sum of the plant transpiration and the water lost without being used by the plant (evaporation) (Flexas et al., 2010). To make agriculture more effective the second component has to become smaller. The P-M equation gives only the combined evapotranspiration, which makes it difficult to distinguish between water used by plants and surplus water. Therefore, the water loss is estimated using the combined ET (Zhang et al., 2004). High values of WUE indicate that the vegetation was effectively using most of the available moisture (Glenn et al., 2007; Huxman et al., 2004). This was the case in spring and autumn during the study period, in summer the values were in general lower in the whole study area, except for one high value in mid August (Figure 3.13a & b). The lower values in summer can be due to higher soil evaporation as most of the crops have been harvested or not grown yet (Hu et al., 2013). Therefore an effective way to reduce ET and hence increase WUE would be to decrease soil evaporation (Zhang et al., 2004).

The WUE modelled here is within the value range found in literature. However, the range is very wide. As both ET and GPP proved to be estimated accurately for the study area, the WUE can also be expected to be reliable. Due to the division used to calculate the WUE, it is very sensitive to low ET values. For a better performance a threshold for ET values close to 0 could be used.

4.3 Added Value of the Performance Indicators

Most performance indicators (PI) developed in studies are either related to financial values such as profit gained from yield and effectiveness of different parts of the production (Elnmer et al., 2018) or are used to compare different parameters and approaches (Alexandridis et al., 2014). The approach in this thesis, to use PI to simplify complex scientific data for a more general user, is hardly used in scientific papers. There are some websites similar to the app created here, such as Fruitlook.co.za (2020) which shows the calculated parameters such as LAI directly and does not have additional PI which further use this data to illustrate yield, for example. The here developed PI and their respective adaptable graphics use the calculated parameters, and some additional information if necessary, to interpret the data in an easy way. Instead of using complicated statistics, the same is shown in adaptable graphics for the respective PI (Figures 3.17, 3.19, 3.21).

For each PI only a few fields were classified in the highest category (Table 3.1). This means that most of the fields have room for improvement in the respective PI. However, this could also be a product of the classification of the study area. The crop type classes are a mixture of different crops and possibly dirt roads and bare soil. The fields, on the other hand, are homogeneous and, therefore more representative for the crop type. This could also be a reason why the two fields belonging to the mixed crop class are in the highest category in the yield and water use PI. The summer crop field can be found in the middle class for two of the three indicators. This is also the crop class which was classified most reliably and hence the area of this class is most homogeneous. The fields of the winter crop class are situated in the middle and low categories, except for field 5 in the yield PI. This can be due to the difficulties in distinguishing between the winter crop and mixed crop classes. The area used to compare the test fields with, were probably not homogeneous enough for a real comparison.

Most of the test fields are classified in the middle category of the water use PI. This could indicate that the range of values falling into this category is too wide and not the same thresholds as for the yield PI can be used. In contrast 2 fields fall in each category in the yield PI, which shows that the threshold values are appropriate for this parameter. That no field was classified into the highest and intermediate productivity category can be explained by the fact that the same area of 50 ha was used for all fields. In reality, all fields have a different size which is unknown since no field measurements were conducted. However, if the tool were used by farmers, they would have to register their fields with the correct size. It is expected that this PI would work better if the exact area were known.

4.4 Outlook

After analysing the created base maps and the developed app, some issues and error sources were detected. How the used methods can be improved is discussed in the following section.

4.4.1 Advancement of Base Maps

A higher spatial resolution of the input data would be helpful in order to be able to model the different parameters more accurately and hence produce more reliable base maps. Using for instance a drone instead of satellite imagery, would lead to a more accurate representation of the fields and enables the identification of patterns due to water loss within each field. All variables which were not generated from the Sentinel-2 images (resolution of 10 m) were only available at one location and assumed to be constant over the whole study area. Therefore, the fields nearest to those stations have more precisely modelled values. On the other hand, this approach reflects reality better as not every farmer has their own meteorological station for the fields. Using this method showed that modelling ET and GPP with these constant values is possible, with the result not being as accurate as it could be.

Another important area where improvements can be made is the classification. As this step was considered a necessity for the results but was not the main focus of this thesis, a very simple approach was used. Due to this, the three resulting classes are not clearly distinguishable crops but rather crop types or mixtures of different crops. To be able to make a better classification, another method can be used where additional field measurements are utilized to validate the result. This would help to make the interpretation of the results easier and more valuable to the end user.

Finally, during this thesis some issues when using the P-M equation were detected. The equation is only meant to be used for vegetated areas, which does not include bare fields. But some of said fields were present, that induced errors in the resulting base maps. Using threshold values and masks of the crop type classes, when applying the P-M equation, could help in preventing these errors. Also some input parameters for the P-M equation are considered to be constant over the study area. However, they could be calculated in a different way for each crop class which could make the resulting ET of the fields more accurate. As mentioned under section 4.2.4 the result of the P-M equation is the combination of the evaporation and transpiration, which makes

it hard to distinguish between water used by plants and surplus water. The partitioning of the modelled ET could therefore lead to a better detection of the location of major water losses in agriculture, whether they are in the soil or the plants themselves. To that, the FloX-Box was installed in April 2019 which makes the data used here, the first to be collected by the sampler. This could lead to not so well calibrated measurements, as there were no reference measurements from another study. This could explain some patterns in the data for which no clear origin can be found.

4.4.2 Making the App more efficient

The functionality of the generated app is limited to the visualisation of the previously modelled and calculated data using MATLAB. To be able to give the user information on any desired input date and year (in the time frame of Sentinel-2), the whole work flow, from downloading the satellite imagery and meteorological data to the processing of the inputs would have to be automated. This leads to some problems such as account-protected web services such as the Copernicus Open Access Hub for Sentinel data and the data service platform IDAWEB of MeteoSwiss as well as the digitisation of the desired fields of the farmers. For the app to be able to execute such complex workflows and time intensive calculation, it may be necessary to use a different tool than R Shiny. One possibility would be to use the Google Earth Engine which meets most of the requirements mentioned here.

For this thesis, three performance indicators were created. With the calculated results and possible user inputs more PI could be created and added to the app. Similar to the field area input for the productivity PI, other data can be provided by the user, such as yields of previous years to use as reference values instead of literature numbers and perhaps to generate trends for future years. It would also be very useful to include the weather forecast from the nearest meteorological station in order to be able to give farmers advice as to when to irrigate the fields to maximise water use efficiency.

5 Conclusion

In this Master thesis, I analysed which parameters and data comparisons can be useful for farmers in their decision making. I investigated how abstract remote sensing data can be visualised for the information to be usable by the target group. I showed the possibilities of presenting the results in an R Shiny app and the limitations of the used methods which can be improved in future research projects.

Four base map parameters (LAI, ET, GPP and WUE) emerged to be useful for the creation of the performance indicators. These performance indicators enable the visualisation of the complex data generated, with for instance the Penman-Monteith equation, in an understandable and interpretable way. The potential yield, water use and productivity can add value to the base map parameters in providing additional information for the farmer's decision-making processes. The usability of the generated PI can be tested further by questioning farmers about the created app using a questionnaire. The feedback gathered therefrom can then be used to come up with a second iteration of PI which may be more suited to the needs of the farmers. One of the biggest limitations encountered during this thesis was the classification of the agricultural fields into different crops. Even when three indices, each using different band combinations, were used, the classification proved to be faulty and combine fields with clearly different crops together in one category. Due to this, the comparison between test fields and their respectable crop classes was prone to error, which may be represented in the results of the PI. As neither the classification nor the creation of perfect parameter base maps were the main aim of this thesis, these errors were left in the resulting data. For a more sophisticated future use of the findings of this thesis, these error sources have to be known and addressed. Multiple studies, each carrying out research on a different input parameter used here, exist today and promise a possible improvement in both the classification and the calculation of the base map parameters.

In spite of the limitations of the methods employed, the approach using performance indicators for the visualisation of complex remote sensing data is very promising. With ongoing research the input parameters can be improved and with that a useful and functioning tool can be developed.

Bibliography

- Alexandridis, T. K., Panagopoulos, A., Galanis, G., Alexiou, I., Cherif, I., Chemin, Y., Stavrinou, E., Bilas, G. & Zalidis, G. C. (2014). Combining remotely sensed surface energy fluxes and GIS analysis of groundwater parameters for irrigation system assessment. *Irrigation Science*, 32(2), 127–140. <https://doi.org/10.1007/s00271-013-0419-8>
- Allen, R., Smith, M., Perrier, A. & Pereira, L. (1994). An update for the definition of reference evapotranspiration. *ICID Bulletin*, 43(2), 1–34.
- Allen, R. G., Pereira, L. S., Raes, D. & Smith, M. (1998). *Crop evapotranspiration : guidelines for computing crop water requirements*. Rome, FAO - Food; Agriculture Organization of the United Nations. <http://www.fao.org/3/X0490E/X0490E00.htm>
- Bandaru, V., West, T. O., Ricciuto, D. M. & César Izaurralde, R. (2013). Estimating crop net primary production using national inventory data and MODIS-derived parameters. *ISPRS Journal of Photogrammetry and Remote Sensing*, 80, 61–71. <https://doi.org/10.1016/j.isprsjprs.2013.03.005>
- Beer, C., Reichstein, M., Tomelleri, E., Ciais, P., Jung, M., Carvalhais, N., Rödenbeck, C., Altaf Arain, M., Baldocchi, D., Bonan, G. B., Bondeau, A., Cescatti, A., Lasslop, G., Lindroth, A., Lomas, M., Luysaert, S., Margolis, H., Oleson, K. W., Rouspard, O., ... Papale, D. (2009). Supporting Online Material Terrestrial Gross Carbon Dioxide Uptake: Global Distribution and Covariation with Climate. *Proc. Natl. Acad. Sci. U.S.A.*, 462(2), 198. <https://doi.org/10.1126/science.1192033>
- Böhler, J. E., Schaepman, M. E. & Kneubühler, M. (2020). Crop Separability from Individual and Combined Airborne Imaging Spectroscopy and UAV Multispectral Data. *Remote Sensing*, 12(8), 1256. <https://doi.org/10.3390/rs12081256>
- Cai, J., Liu, Y., Lei, T. & Pereira, L. S. (2007). Estimating reference evapotranspiration with the FAO Penman-Monteith equation using daily weather forecast messages. *Agricultural and Forest Meteorology*, 145(1-2), 22–35. <https://doi.org/10.1016/j.agrformet.2007.04.012>
- Calanca, P., Smith, P., Pascale Smith, Holzkämper, A. & Ammann, C. (2011). Die Referenzverdunstung und ihre Anwendung in der Agrarmeteorologie. *Agrarforschung Schweiz*, 2(4), 176–183.
- Chartzoulakis, K. & Bertaki, M. (2015). Sustainable Water Management in Agriculture under Climate Change. *Agriculture and Agricultural Science Procedia*, 4, 88–98. <https://doi.org/10.1016/j.aaspro.2015.03.011>
- Chávez, J. L., Neale, C. M., Prueger, J. H. & Kustas, W. P. (2008). Daily evapotranspiration estimates from extrapolating instantaneous airborne remote sensing et values. *Irrigation Science*, 27(1), 67–81. <https://doi.org/10.1007/s00271-008-0122-3>

- Chhabra, R. (1996). *Soil Salinity and Water Quality*. London, Routledge. <https://doi.org/10.1201/9780203739242>
- Coppo, P., Taiti, A., Pettinato, L., Francois, M., Taccola, M. & Drusch, M. (2017). Fluorescence imaging spectrometer (FLORIS) for ESA FLEX mission. *Remote Sensing*, 9(7), 649. <https://doi.org/10.3390/rs9070649>
- Damm, A., Guanter, L., Paul-Limoges, E., van der Tol, C., Hueni, A., Buchmann, N., Eugster, W., Ammann, C. & Schaepman, M. E. (2015). Far-red sun-induced chlorophyll fluorescence shows ecosystem-specific relationships to gross primary production: An assessment based on observational and modeling approaches. *Remote Sensing of Environment*, 166, 91–105. <https://doi.org/10.1016/j.rse.2015.06.004>
- de Carvalho, L. G., Evangelista, A. W. P., Oliveira, K. M. G., Silva, B. M., Alves, M. D. C., de Sá Júnior, A. & Miranda, W. L. (2013). FAO Penman-Monteith equation for reference evapotranspiration from missing data. *Idesia*, 31(3), 39–47. <https://doi.org/10.4067/S0718-34292013000300006>
- Degreen & Locusta. (2020). Solar radiation. https://de.wikipedia.org/wiki/Sonnenstrahlung#/media/Datei:Sonne_Strahlungsintensitaet.svg
- Delegido, J., Verrelst, J., Meza, C. M., Rivera, J. P., Alonso, L. & Moreno, J. (2013). A red-edge spectral index for remote sensing estimation of green LAI over agroecosystems. *European Journal of Agronomy*, 46, 42–52. <https://doi.org/10.1016/j.eja.2012.12.001>
- Drusch, M., Del Bello, U., Carlier, S., Colin, O., Fernandez, V., Gascon, F., Hoersch, B., Isola, C., Laberinti, P., Martimort, P., Meygret, A., Spoto, F., Sy, O., Marchese, F. & Bargellini, P. (2012). Sentinel-2: ESA's Optical High-Resolution Mission for GMES Operational Services. *Remote Sensing of Environment*, 120, 25–36. <https://doi.org/10.1016/j.rse.2011.11.026>
- D'Urso, G. & Belmonte, A. C. (2006). Operative approaches to determine crop water requirements from earth observation data: Methodologies and applications, In *Aip conference proceedings*. <https://doi.org/10.1063/1.2349323>
- Elnmer, A., Khadr, M., Allam, A., Kanae, S. & Tawfik, A. (2018). Assessment of irrigation water performance in the Nile delta using remotely sensed data. *Water (Switzerland)*, 10(10), 1375. <https://doi.org/10.3390/w10101375>
- ESA. (2015). Sentinel-2 User Handbook. *ESA Standard Document*, (1), 64.
- Falkenmark, M. (2013). Growing water scarcity in agriculture: Future challenge to global water security. *Philosophical Transactions of the Royal Society A: Mathematical, Physical and Engineering Sciences*, 371(2002). <https://doi.org/10.1098/rsta.2012.0410>
- Falloon, P. & Betts, R. (2010). Climate impacts on European agriculture and water management in the context of adaptation and mitigation-The importance of an integrated approach. *Science of the Total Environment*, 408(23), 5667–5687. <https://doi.org/10.1016/j.scitotenv.2009.05.002>
- Farahani, H. J. & Bausch, W. C. (1995). Performance of evapotranspiration models for maize - Bare soil to closed canopy. *Transactions of the American Society of Agricultural Engineers*, 38(4), 1049–1059. <https://doi.org/10.13031/2013.27922>
- Farg, E., Arafat, S., Abd El-Wahed, M. S. & El-Gindy, A. (2017). Evaluation of water distribution under pivot irrigation systems using remote sensing imagery in eastern Nile delta. *Egypt-*

- tian Journal of Remote Sensing and Space Science*, 20, S13–S19. <https://doi.org/10.1016/j.ejrs.2016.12.001>
- Fisher, J. B., Melton, F., Middleton, E., Hain, C., Anderson, M., Allen, R., McCabe, M. F., Hook, S., Baldocchi, D., Townsend, P. A., Kilic, A., Tu, K., Miralles, D. D., Perret, J., Lagouarde, J. P., Waliser, D., Purdy, A. J., French, A., Schimel, D., ... Wood, E. F. (2017). The future of evapotranspiration: Global requirements for ecosystem functioning, carbon and climate feedbacks, agricultural management, and water resources. *Water Resources Research*, 53(4), 2618–2626. <https://doi.org/10.1002/2016WR020175>
- Fisher, J. B., Tu, K. P. & Baldocchi, D. D. (2008). Global estimates of the land-atmosphere water flux based on monthly AVHRR and ISLSCP-II data, validated at 16 FLUXNET sites. *Remote Sensing of Environment*, 112(3), 901–919. <https://doi.org/10.1016/j.rse.2007.06.025>
- Flexas, J., GalmaS, J., Galla, A., Gulaias, J., Pou, A., Ribas-Carbo, M., TomaS, M. & Medrano, H. (2010). Improving water use efficiency in grapevines: potential physiological targets for biotechnological improvement. *Australian Journal of Grape and Wine Research*, 16(SUPPL. 1), 106–121. <https://doi.org/10.1111/j.1755-0238.2009.00057.x>
- Fruitlook. (2020). <https://www.fruitlook.co.za/>
- Garcia, M., Raes, D., Allen, R. & Herbas, C. (2004). Dynamics of reference evapotranspiration in the Bolivian highlands (Altiplano). *Agricultural and Forest Meteorology*, 125(1-2), 67–82. <https://doi.org/10.1016/j.agrformet.2004.03.005>
- Gavilán, P., Lorite, I. J., Tornero, S. & Berengena, J. (2006). Regional calibration of Hargreaves equation for estimating reference et in a semiarid environment. *Agricultural Water Management*, 81(3), 257–281. <https://doi.org/10.1016/j.agwat.2005.05.001>
- Glenn, E. P., Huete, A. R., Nagler, P. L., Hirschboeck, K. K. & Brown, P. (2007). Integrating remote sensing and ground methods to estimate evapotranspiration. <https://doi.org/10.1080/07352680701402503>
- González, J. A. & Calbó, J. (2002). Modelled and measured ratio of PAR to global radiation under cloudless skies. *Agricultural and Forest Meteorology*, 110(4), 319–325. [https://doi.org/10.1016/S0168-1923\(01\)00291-X](https://doi.org/10.1016/S0168-1923(01)00291-X)
- Grassland Sciences. (2020). <https://gl.ethz.ch/>
- Hegerl, G., F. W. Zwiers, Braconnot, P., Gillett, N., Luo, Y., Orsini, J. M., Nicholls, N., Penner, J. & Stott, P. (2007). *Understanding and Attributing Climate Change. In: Climate Change 2007: The Physical Science Basis. Contribution of Working Group I to the Fourth Assessment Report of the Intergovernmental Panel on Climate Change* (tech. rep. No. 3-4). Cambridge University Press. <https://doi.org/10.1007/s10584-006-9107-5>
- Hu, Z., Li, S., Yu, G., Sun, X., Zhang, L., Han, S. & Li, Y. (2013). Modeling evapotranspiration by combing a two-source model, a leaf stomatal model, and a light-use efficiency model. *Journal of Hydrology*, 501, 186–192. <https://doi.org/10.1016/j.jhydrol.2013.08.006>
- Huete, A., Didan, K., Miura, T., Rodriguez, E. P., Gao, X. & Ferreira, L. G. (2002). Overview of the radiometric and biophysical performance of the MODIS vegetation indices. *Remote Sensing of Environment*, 83(1-2), 195–213. [https://doi.org/10.1016/S0034-4257\(02\)00096-2](https://doi.org/10.1016/S0034-4257(02)00096-2)
- Hunt, E. R., Doraiswamy, P. C., McMurtrey, J. E., Daughtry, C. S., Perry, E. M. & Akhmedov, B. (2012). A visible band index for remote sensing leaf chlorophyll content at the Canopy

- scale. *International Journal of Applied Earth Observation and Geoinformation*, 21(1), 103–112. <https://doi.org/10.1016/j.jag.2012.07.020>
- Huxman, T. E., Smith, M. D., Fay, P. A., Knapp, A. K., Shaw, M. R., Lolk, M. E., Smith, S. D., Tissue, D. T., Zak, J. C., Weltzin, J. F., Pockman, W. T., Sala, O. E., Haddad, B. M., Harte, J., Koch, G. W., Schwinning, S., Small, E. E. & Williams, D. G. (2004). Convergence across biomes to a common rain-use efficiency. *Nature*, 429(6992), 651–654. <https://doi.org/10.1038/nature02561>
- Irmak, S., Djaman, K. & Rudnick, D. R. (2016). Effect of full and limited irrigation amount and frequency on subsurface drip-irrigated maize evapotranspiration, yield, water use efficiency and yield response factors. *Irrigation Science*, 34(4), 271–286. <https://doi.org/10.1007/s00271-016-0502-z>
- Jewell, J. (2011). *The IEA Model of Short-term Energy Security (MOSES) - Primary Energy Sources and Secondary Fuels* (tech. rep.). International Energy Agency. <https://doi.org/10.1787/5k9h0wd2ghlv-en>
- Karam, F., Lahoud, R., Masaad, R., Kabalan, R., Breidi, J., Chalita, C. & Rouphael, Y. (2007). Evapotranspiration, seed yield and water use efficiency of drip irrigated sunflower under full and deficit irrigation conditions. *Agricultural Water Management*, 90(3), 213–223. <https://doi.org/10.1016/j.agwat.2007.03.009>
- Kodur, S., Shrestha, U. B., Maraseni, T. N. & Deo, R. C. (2019). Environmental and economic impacts and trade-offs from simultaneous management of soil constraints, nitrogen and water. *Journal of Cleaner Production*, 222, 960–970. <https://doi.org/10.1016/j.jclepro.2019.03.079>
- Kruse, F. A., Lefkoff, A. B., Boardman, J. W., Heidebrecht, K. B., Shapiro, A. T., Barloon, P. J. & Goetz, A. F. H. (1993). The spectral image processing system (SIPS)-interactive visualization and analysis of imaging spectrometer data, In *American journal of physics*. <https://doi.org/10.1063/1.44433>
- landwirtschaft.ch. (2020). <https://www.landwirtschaft.ch/wissen-facts/produktion/ackerbau/>
- Laurent, V. C., Verhoef, W., Damm, A., Schaepman, M. E. & Clevers, J. G. (2013). A Bayesian object-based approach for estimating vegetation biophysical and biochemical variables from APEX at-sensor radiance data. *Remote Sensing of Environment*, 139, 6–17. <https://doi.org/10.1016/j.rse.2013.07.032>
- Lehner, B., Döll, P., Alcamo, J., Henrichs, T. & Kaspar, F. (2006). Estimating the impact of global change on flood and drought risks in Europe: A continental, integrated analysis. *Climatic Change*, 75(3), 273–299. <https://doi.org/10.1007/s10584-006-6338-4>
- Li, X., Xiao, J., He, B., Altaf Arain, M., Beringer, J., Desai, A. R., Emmel, C., Hollinger, D. Y., Krasnova, A., Mammarella, I., Noe, S. M., Ortiz, P. S., Rey-Sanchez, A. C., Rocha, A. V. & Varlagin, A. (2018). Solar-induced chlorophyll fluorescence is strongly correlated with terrestrial photosynthesis for a wide variety of biomes: First global analysis based on OCO-2 and flux tower observations. *Global Change Biology*, 24(9), 3990–4008. <https://doi.org/10.1111/gcb.14297>
- Lillesand, T. M., Kiefer, R. W. & Chipman, J. W. (2015). *Remote Sensing and Image Interpretation* (Seventh ed). Wiley.

- Lin, S., Li, J., Liu, Q., Li, L., Zhao, J. & Yu, W. (2019). Evaluating the effectiveness of using vegetation indices based on red-edge reflectance from Sentinel-2 to estimate gross primary productivity. *Remote Sensing*, 11(11), 25. <https://doi.org/10.3390/rs11111303>
- Louhaichi, M., Borman, M. M. & Johnson, D. E. (2001). Spatially located platform and aerial photography for documentation of grazing impacts on wheat. *Geocarto International*, 16(1), 65–70. <https://doi.org/10.1080/10106040108542184>
- Lui, J. & Yang, H. (2010). Global agricultural green and blue water consumptive uses and virtual water trade, In *Rethinking water and food security*. Leyden, The Netherlands, CRC Press. <https://doi.org/10.1201/b10541>
- Masek, J. G., Hayes, D. J., Joseph Hughes, M., Healey, S. P. & Turner, D. P. (2015). The role of remote sensing in process-scaling studies of managed forest ecosystems. *Forest Ecology and Management*, 355, 109–123. <https://doi.org/10.1016/j.foreco.2015.05.032>
- Mo, X., Liu, S., Lin, Z., Xu, Y., Xiang, Y. & McVicar, T. R. (2005). Prediction of crop yield, water consumption and water use efficiency with a SVAT-crop growth model using remotely sensed data on the North China Plain. *Ecological Modelling*, 183(2-3), 301–322. <https://doi.org/10.1016/j.ecolmodel.2004.07.032>
- Monteith, J. L. (1972). Solar Radiation and Productivity in Tropical Ecosystems. *The Journal of Applied Ecology*, 9(3), 747. <https://doi.org/10.2307/2401901>
- Monteith, J. L. (1977). *Climate and the efficiency of crop production in Britain* (tech. rep.).
- Oensingen site. (2020). <https://www.swissfluxnet.ethz.ch/index.php/sites/ch-oe2-oensingen/site-info-ch-oe2/>
- Oki, T. & Kanae, S. (2006). Global hydrological cycles and world water resources. <https://doi.org/10.1126/science.1128845>
- Paul-Limoges, E., Damm, A., Hueni, A., Liebisch, F., Eugster, W., Schaepman, M. E. & Buchmann, N. (2018). Effect of environmental conditions on sun-induced fluorescence in a mixed forest and a cropland. *Remote Sensing of Environment*, 219, 310–323. <https://doi.org/10.1016/j.rse.2018.10.018>
- Paul-Limoges, E., Wolf, S., Schneider, F. D., Longo, M., Moorcroft, P., Gharun, M. & Damm, A. (2020). Partitioning evapotranspiration with concurrent eddy covariance measurements in a mixed forest. *Agricultural and Forest Meteorology*, 280, 107786. <https://doi.org/10.1016/j.agrformet.2019.107786>
- Penning de Vries, F., Jansen, D., ten Berge, H. & Bakema, A. (1989). *Simulation of ecophysiological processes of growth in several annual crops*. Wageningen, The Netherlands, Pudoc.
- Qiu, G. Y., Wang, L., He, X., Zhang, X., Chen, S., Chen, J. & Yang, Y. (2008). Water use efficiency and evapotranspiration of winter wheat and its response to irrigation regime in the north China plain. *Agricultural and Forest Meteorology*, 148(11), 1848–1859. <https://doi.org/10.1016/j.agrformet.2008.06.010>
- Reichstein, M., Falge, E., Baldocchi, D., Papale, D., Aubinet, M., Berbigier, P., Bernhofer, C., Buchmann, N., Gilmanov, T., Granier, A., Grünwald, T., Havránková, K., Ilvesniemi, H., Janous, D., Knohl, A., Laurila, T., Lohila, A., Loustau, D., Matteucci, G., ... Valentini, R. (2005). On the separation of net ecosystem exchange into assimilation and ecosystem respiration: Re-

- view and improved algorithm. John Wiley & Sons, Ltd. <https://doi.org/10.1111/j.1365-2486.2005.001002.x>
- Reville, A., Emmel, C., D'Odorico, P., Buchmann, N., Hörtnagl, L. & Eugster, W. (2019). Estimating cropland carbon fluxes: A process-based model evaluation at a Swiss crop-rotation site. *Field Crops Research*, 234(April 2018), 95–106. <https://doi.org/10.1016/j.fcr.2019.02.006>
- Riley, W. J., Ortiz-Monasterio, I. & Matson, P. A. (2001). Nitrogen leaching and soil nitrate, nitrite, and ammonium levels under irrigated wheat in Northern Mexico. *Nutrient Cycling in Agroecosystems*, 61(3), 223–236. <https://doi.org/10.1023/A:1013758116346>
- Rodrigues, D. B., Gupta, H. V. & Mendiondo, E. M. (2014). A blue/green water-based accounting framework for assessment of water security. *Water Resources Research*, 50(9), 7187–7205. <https://doi.org/10.1002/2013WR014274>
- Rosegrant, M. W., Ringler, C. & Zhu, T. (2009). Water for Agriculture: Maintaining Food Security under Growing Scarcity. *Annual Review of Environment and Resources*, 34(1), 205–222. <https://doi.org/10.1146/annurev.envIRON.030308.090351>
- RStudio, I. (2020). Easy web applications in R. <https://shiny.rstudio.com/>
- Schaepman, M. E., Jehle, M., Hueni, A., D'Odorico, P., Damma, A., Weyermann, J., Schneider, F. D., Laurent, V., Popp, C., Seidel, F. C., Lenhard, K., Gege, P., Kuchler, C., Brazile, J., Kohler, P., De Vos, L., Meuleman, K., Meynart, R., Schläpfer, D., ... Itten, K. I. (2015). Advanced radiometry measurements and Earth science applications with the Airborne Prism Experiment (APEX). *Remote Sensing of Environment*, 158(1), 207–219. <https://doi.org/10.1016/j.rse.2014.11.014>
- Schuol, J., Abbaspour, K. C., Srinivasan, R. & Yang, H. (2008). Estimation of freshwater availability in the West African sub-continent using the SWAT hydrologic model. *Journal of Hydrology*, 352(1-2), 30–49. <https://doi.org/10.1016/j.jhydrol.2007.12.025>
- Schyns, J. F., Hoekstra, A. Y. & Booij, M. J. (2015). Review and classification of indicators of green water availability and scarcity. *Hydrology and Earth System Sciences*, 19(11), 4581–4608. <https://doi.org/10.5194/hess-19-4581-2015>
- Suyker, A. E., Verma, S. B., Burba, G. G. & Arkebauer, T. J. (2005). Gross primary production and ecosystem respiration of irrigated maize and irrigated soybean during a growing season. *Agricultural and Forest Meteorology*, 131(3-4), 180–190. <https://doi.org/10.1016/j.agrformet.2005.05.007>
- Swiss Granum. (2017). Getreide , Ölsaaten und Körnerleguminosen Schätzung Anbauflächen von Wintergetreide und Raps. *Bericht Schweizerische Branchenorganisation Getreide*, 1, 1–6.
- Tian, H., Chen, G., Liu, M., Zhang, C., Sun, G., Lu, C., Xu, X., Ren, W., Pan, S. & Chappelka, A. (2010). Model estimates of net primary productivity, evapotranspiration, and water use efficiency in the terrestrial ecosystems of the southern United States during 1895-2007. *Forest Ecology and Management*, 259(7), 1311–1327. <https://doi.org/10.1016/j.foreco.2009.10.009>
- Vanino, S., Nino, P., De Michele, C., Falanga Bolognesi, S., D'Urso, G., Di Bene, C., Pennelli, B., Vuolo, F., Farina, R., Pulighe, G. & Napoli, R. (2018). Capability of Sentinel-2 data for estimating maximum evapotranspiration and irrigation requirements for tomato crop in Central

- Italy. *Remote Sensing of Environment*, 215, 452–470. <https://doi.org/10.1016/j.rse.2018.06.035>
- Veettil, A. V. & Mishra, A. K. (2016). Water security assessment using blue and green water footprint concepts. *Journal of Hydrology*, 542, 589–602. <https://doi.org/10.1016/j.jhydrol.2016.09.032>
- Velthof, G. L., Lesschen, J. P., Webb, J., Pietrzak, S., Miatkowski, Z., Pinto, M., Kros, J. & Oenema, O. (2014). The impact of the Nitrates Directive on nitrogen emissions from agriculture in the EU-27 during 2000-2008. *Science of the Total Environment*, 468-469, 1225–1233. <https://doi.org/10.1016/j.scitotenv.2013.04.058>
- Viña, A., Gitelson, A. A., Nguy-Robertson, A. L. & Peng, Y. (2011). Comparison of different vegetation indices for the remote assessment of green leaf area index of crops. *Remote Sensing of Environment*, 115(12), 3468–3478. <https://doi.org/10.1016/j.rse.2011.08.010>
- Vincini, M., Frazzi, E. & D'Alessio, P. (2008). A broad-band leaf chlorophyll vegetation index at the canopy scale, In *Precision agriculture*, Springer US. <https://doi.org/10.1007/s11119-008-9075-z>
- Wei, S., Yi, C., Fang, W. & Hendrey, G. (2017). A global study of GPP focusing on light-use efficiency in a random forest regression model. *Ecosphere*, 8(5). <https://doi.org/10.1002/ecs2.1724>
- Weyermann, J., Schläpfer, D., Hueni, A., Kneubühler, M. & Schaepman, M. (2009). Spectral Angle Mapper (SAM) for anisotropy class indexing in imaging spectrometry data. *Imaging Spectrometry XIV*, 7457(August 2009), 74570B. <https://doi.org/10.1117/12.825991>
- Wolanin, A., Camps-Valls, G., Gómez-Chova, L., Mateo-García, G., van der Tol, C., Zhang, Y. & Guanter, L. (2019). Estimating crop primary productivity with Sentinel-2 and Landsat 8 using machine learning methods trained with radiative transfer simulations. *Remote Sensing of Environment*, 225, 441–457. <https://doi.org/10.1016/j.rse.2019.03.002>
- WWAP, U. N. W. W. A. P. (2014). The United Nations World Water Development Report 2014: Water and Energy. UNESCO.
- Xiao, X., Zhang, Q., Hollinger, D., Aber, J. & Berrien, M. (2005). Modeling gross primary production of an evergreen needleleaf forest using modis and climate data. *Ecological Applications*, 15(3), 954–969. <https://doi.org/10.1890/04-0470>
- Xin, Q., Broich, M., Suyker, A. E., Yu, L. & Gong, P. (2015). Multi-scale evaluation of light use efficiency in MODIS gross primary productivity for croplands in the Midwestern United States. *Agricultural and Forest Meteorology*, 201, 111–119. <https://doi.org/10.1016/j.agrformet.2014.11.004>
- Zhang, Y., Kendy, E., Qiang, Y., Changming, L., Yanjun, S. & Hongyong, S. (2004). Effect of soil water deficit on evapotranspiration, crop yield, and water use efficiency in the North China Plain. *Agricultural Water Management*, 64(2), 107–122. [https://doi.org/10.1016/S0378-3774\(03\)00201-4](https://doi.org/10.1016/S0378-3774(03)00201-4)

A Appendix - Additional Figures and Tables

TABLE A.1: Daily mean leaf area index with the standard deviation indicated for the whole study area, the three crop type classes and the six test fields.

Date	Area	Summer Crop	Mixed Crop	Winter Crop	Field 1	Field 2	Field 3	Field 4	Field 5	Field 6
20.04.2019	2.5 ± 1.0	0.5 ± 1.2	1.3 ± 1.5	0.6 ± 1.1	3.0 ± 0.4	3.7 ± 0.1	3.4 ± 0.4	1.7 ± 0.6	2.7 ± 1.2	3.1 ± 0.4
04.06.2019	2.2 ± 1.1	0.1 ± 0.4	1.4 ± 1.5	0.7 ± 1.2	3.4 ± 0.3	3.4 ± 0.1	0.1 ± 0.9	2.3 ± 0.9	2.8 ± 1.0	3.0 ± 0.3
19.06.2019	1.9 ± 1.0	0.2 ± 0.6	1.1 ± 1.3	0.6 ± 1.0	2.0 ± 0.3	0.3 ± 0.1	0.3 ± 0.1	1.8 ± 0.7	2.1 ± 0.9	2.6 ± 0.2
29.06.2019	1.7 ± 0.9	0.3 ± 0.7	0.9 ± 1.1	0.5 ± 0.9	2.1 ± 0.3	0.1 ± 0.0	1.1 ± 0.3	1.6 ± 0.5	1.2 ± 0.9	1.6 ± 0.5
04.07.2019	1.5 ± 0.8	0.4 ± 0.7	0.8 ± 1.0	0.4 ± 0.7	2.0 ± 0.3	0.1 ± 0.0	1.6 ± 0.2	1.3 ± 0.4	1.2 ± 0.9	0.8 ± 0.6
24.07.2019	1.1 ± 0.8	0.4 ± 0.7	0.6 ± 0.9	0.1 ± 0.4	1.2 ± 0.2	0.6 ± 0.2	1.6 ± 0.1	0.2 ± 0.2	1.0 ± 0.8	0.4 ± 0.6
08.08.2019	1.6 ± 1.0	0.5 ± 0.9	0.9 ± 1.2	0.2 ± 0.6	2.5 ± 0.4	3.7 ± 0.1	2.2 ± 0.2	0.3 ± 0.4	1.7 ± 1.0	0.7 ± 1.1
18.08.2019	1.8 ± 1.2	0.5 ± 1.0	1.0 ± 1.4	0.3 ± 0.7	3.0 ± 0.4	1.1 ± 0.1	1.9 ± 0.3	0.5 ± 0.9	2.4 ± 0.9	1.1 ± 1.5
28.08.2019	1.9 ± 1.1	0.6 ± 1.0	1.1 ± 1.4	0.2 ± 0.7	2.9 ± 0.5	1.9 ± 0.2	1.9 ± 0.3	0.6 ± 0.2	2.7 ± 1.1	0.8 ± 1.2
12.09.2019	2.3 ± 1.1	0.6 ± 1.0	1.6 ± 1.6	0.2 ± 0.5	2.9 ± 0.4	3.7 ± 0.1	0.1 ± 0.1	1.1 ± 0.6	2.2 ± 1.2	0.9 ± 1.2
12.10.2019	2.1 ± 1.2	0.3 ± 0.7	1.4 ± 1.5	0.4 ± 0.9	3.1 ± 0.3	2.1 ± 0.1	0.3 ± 0.2	2.2 ± 1.3	2.8 ± 0.9	2.7 ± 0.4

TABLE A.2: Daily mean evapotranspiration [mm/day] with the standard deviation indicated for the whole study area, the three crop type classes and the six test fields.

Date	Area	Summer Crop	Mixed Crop	Winter Crop	Field 1	Field 2	Field 3	Field 4	Field 5	Field 6
20.04.2019	4.8 ± 0.8	4.4 ± 1.2	4.9 ± 0.5	4.8 ± 0.7	5.0 ± 0.1	5.1 ± 0.0	5.0 ± 0.2	4.7 ± 0.7	4.7 ± 0.9	5.1 ± 0.1
04.06.2019	6.9 ± 1.1	5.6 ± 1.7	7.2 ± 0.2	7.2 ± 0.4	7.2 ± 0.0	7.4 ± 0.0	3.0 ± 1.6	7.2 ± 0.5	7.1 ± 0.3	7.4 ± 0.1
19.06.2019	6.6 ± 1.3	5.2 ± 1.8	7.0 ± 0.5	7.0 ± 0.8	7.0 ± 0.2	4.5 ± 0.5	4.4 ± 0.8	7.0 ± 0.8	6.8 ± 0.5	7.0 ± 0.1
29.06.2019	7.5 ± 1.1	6.9 ± 1.4	7.8 ± 1.0	7.7 ± 1.0	8.0 ± 0.2	2.3 ± 0.9	7.6 ± 0.6	8.0 ± 0.5	6.8 ± 1.4	7.7 ± 0.3
04.07.2019	6.8 ± 1.1	6.6 ± 1.1	6.91 ± 1.0	6.8 ± 1.1	7.3 ± 0.2	1.4 ± 0.7	7.3 ± 0.1	7.0 ± 0.9	5.8 ± 1.9	5.9 ± 0.8
24.07.2019	6.2 ± 1.8	7.0 ± 1.1	6.4 ± 1.8	4.9 ± 1.9	7.1 ± 0.4	6.3 ± 0.3	7.4 ± 0.1	3.9 ± 1.7	6.0 ± 2.0	3.5 ± 2.0
08.08.2019	5.7 ± 1.3	6.2 ± 0.6	5.8 ± 1.3	5.0 ± 1.6	6.5 ± 0.1	6.2 ± 0.0	6.5 ± 0.1	4.1 ± 1.3	6.1 ± 0.4	3.7 ± 1.9
18.08.2019	5.1 ± 1.5	5.7 ± 0.8	5.3 ± 1.3	4.1 ± 1.8	6.1 ± 0.1	5.2 ± 0.1	5.9 ± 0.4	2.8 ± 1.6	5.8 ± 0.6	3.0 ± 2.4
28.08.2019	5.3 ± 0.9	5.6 ± 0.5	5.6 ± 0.4	4.5 ± 1.3	5.7 ± 0.1	5.7 ± 0.0	5.7 ± 0.1	4.9 ± 0.3	5.6 ± 0.3	3.2 ± 1.8
12.09.2019	4.7 ± 0.8	4.8 ± 0.4	4.9 ± 0.1	3.8 ± 1.3	4.9 ± 0.2	4.8 ± 0.0	1.6 ± 1.0	4.2 ± 1.1	4.8 ± 0.2	2.8 ± 1.8
12.10.2019	2.0 ± 0.5	1.7 ± 0.6	2.2 ± 0.2	1.8 ± 0.5	2.2 ± 0.0	2.2 ± 0.0	1.3 ± 0.3	1.9 ± 0.6	2.1 ± 0.2	2.2 ± 0.0

TABLE A.3: Daily mean gross primary production [g C/m² day] with the standard deviation indicated for the whole study area, the three crop types and the six test fields.

Date	Area	Summer Crop	Mixed Crop	Winter Crop	Field 1	Field 2	Field 3	Field 4	Field 5	Field 6
20.04.2019	13.2 ± 3.8	12.8 ± 5.1	13.6 ± 3.2	12.7 ± 3.4	15.6 ± 0.7	16.9 ± 0.5	16.5 ± 0.9	12.1 ± 1.6	15.2 ± 2.4	15.2 ± 1.4
04.06.2019	13.7 ± 5.0	6.6 ± 3.7	15.8 ± 3.2	15.2 ± 3.3	17.8 ± 0.6	15.7 ± 0.5	2.7 ± 0.7	15.1 ± 2.0	17.2 ± 2.9	17.2 ± 0.9
19.06.2019	11.7 ± 4.4	7.4 ± 4.3	13.4 ± 3.6	12.7 ± 3.1	12.0 ± 0.7	4.0 ± 0.2	4.6 ± 0.3	12.7 ± 1.4	15.3 ± 3.7	16.0 ± 0.6
29.06.2019	11.6 ± 4.0	10.5 ± 4.2	12.3 ± 4.1	11.2 ± 3.3	13.6 ± 0.8	3.4 ± 0.2	11.1 ± 0.8	10.9 ± 1.0	10.0 ± 3.6	12.0 ± 1.7
04.07.2019	10.6 ± 3.9	11.3 ± 3.9	11.3 ± 4.1	8.9 ± 3.0	13.3 ± 0.9	2.8 ± 0.2	14.0 ± 0.7	7.7 ± 0.8	9.6 ± 3.7	7.1 ± 2.7
24.07.2019	9.5 ± 4.4	11.8 ± 3.6	9.2 ± 4.0	5.5 ± 3.3	9.0 ± 0.9	7.1 ± 0.8	14.4 ± 0.6	3.9 ± 0.2	8.6 ± 3.3	5.1 ± 3.0
08.08.2019	9.2 ± 4.3	11.5 ± 3.0	9.6 ± 4.3	6.0 ± 3.5	11.1 ± 0.9	18.2 ± 0.3	13.5 ± 0.4	3.6 ± 1.6	9.9 ± 3.5	5.7 ± 4.9
18.08.2019	9.1 ± 4.3	11.0 ± 2.8	9.6 ± 4.3	6.2 ± 4.0	12.3 ± 0.9	5.5 ± 0.3	12.0 ± 0.4	4.1 ± 3.1	10.8 ± 2.0	6.3 ± 5.9
28.08.2019	8.4 ± 3.7	10.2 ± 2.4	9.1 ± 3.3	5.2 ± 3.6	11.1 ± 1.6	7.7 ± 0.5	10.9 ± 0.4	3.7 ± 0.5	11.6 ± 2.5	4.3 ± 4.2
12.09.2019	9.1 ± 3.2	9.4 ± 2.3	10.7 ± 2.0	4.8 ± 2.5	10.7 ± 0.9	14.1 ± 0.3	1.4 ± 0.3	5.4 ± 1.8	8.5 ± 3.1	4.3 ± 3.8
12.10.2019	4.9 ± 2.4	3.2 ± 2.0	6.2 ± 1.7	4.1 ± 2.3	6.7 ± 0.3	4.3 ± 0.2	1.8 ± 0.2	4.7 ± 1.9	6.7 ± 1.3	5.6 ± 0.7

TABLE A.4: Daily mean water use efficiency [g C/kg H₂O] with the standard deviation indicated for the whole study area, the three crop type classes and the six test fields.

Date	Area	Summer Crop	Mixed Crop	Winter Crop	Field 1	Field 2	Field 3	Field 4	Field 5	Field 6
20.04.2019	3.1 ± 20.6	3.7 ± 41.3	2.9 ± 7.1	2.8 ± 6.8	3.1 ± 0.1	3.3 ± 0.1	3.3 ± 0.1	2.8 ± 1.2	3.6 ± 3.5	3.0 ± 0.2
04.06.2019	2.0 ± 4.8	1.6 ± 10.3	2.2 ± 0.5	2.1 ± 1.0	2.5 ± 0.1	2.1 ± 0.1	2.6 ± 8.8	2.1 ± 0.3	2.4 ± 0.4	2.3 ± 0.1
19.06.2019	1.9 ± 10.0	1.9 ± 18.4	1.9 ± 0.5	1.9 ± 7.4	1.7 ± 0.1	0.9 ± 0.1	1.5 ± 4.3	1.8 ± 0.2	2.1 ± 0.5	2.3 ± 0.1
29.06.2019	1.7 ± 26.9	1.6 ± 5.9	1.8 ± 38.8	1.5 ± 2.2	1.7 ± 0.1	2.1 ± 3.4	1.5 ± 0.1	1.4 ± 0.1	1.6 ± 1.2	1.6 ± 0.2
04.07.2019	1.8 ± 37.1	2.3 ± 71.4	1.7 ± 7.3	1.4 ± 2.5	1.8 ± 0.1	8.9 ± 49.3	1.9 ± 0.1	1.2 ± 0.3	1.9 ± 1.5	1.2 ± 0.3
24.07.2019	1.8 ± 16.9	1.8 ± 6.9	1.6 ± 4.5	2.1 ± 32.8	1.3 ± 0.1	1.1 ± 0.1	1.9 ± 0.1	1.5 ± 2.0	4.6 ± 25.0	2.2 ± 3.8
08.08.2019	1.8 ± 9.0	1.9 ± 2.5	1.8 ± 10.1	1.5 ± 11.4	1.7 ± 0.1	3.0 ± 0.1	2.1 ± 0.0	0.9 ± 0.3	1.6 ± 0.5	2.0 ± 3.7
18.08.2019	2.5 ± 170.7	2.0 ± 4.8	1.9 ± 12.6	4.3 ± 345.1	2.0 ± 0.1	1.1 ± 0.0	2.1 ± 0.2	2.9 ± 7.9	1.9 ± 0.3	2.8 ± 3.6
28.08.2019	1.6 ± 4.2	1.8 ± 1.4	1.6 ± 3.7	1.4 ± 6.4	1.9 ± 0.3	1.4 ± 0.1	1.9 ± 0.1	0.8 ± 0.1	2.1 ± 0.4	2.6 ± 9.6
12.09.2019	2.1 ± 10.90	2.0 ± 1.7	2.1 ± 0.4	2.0 ± 23.5	2.2 ± 0.2	3.0 ± 0.1	3.6 ± 16.5	1.4 ± 0.7	1.8 ± 0.6	2.5 ± 6.0
12.10.2019	2.8 ± 21.6	2.7 ± 35.9	2.9 ± 6.9	2.6 ± 21.2	3.0 ± 0.1	2.0 ± 0.1	0.9 ± 0.3	2.6 ± 1.1	3.1 ± 0.5	2.6 ± 0.3

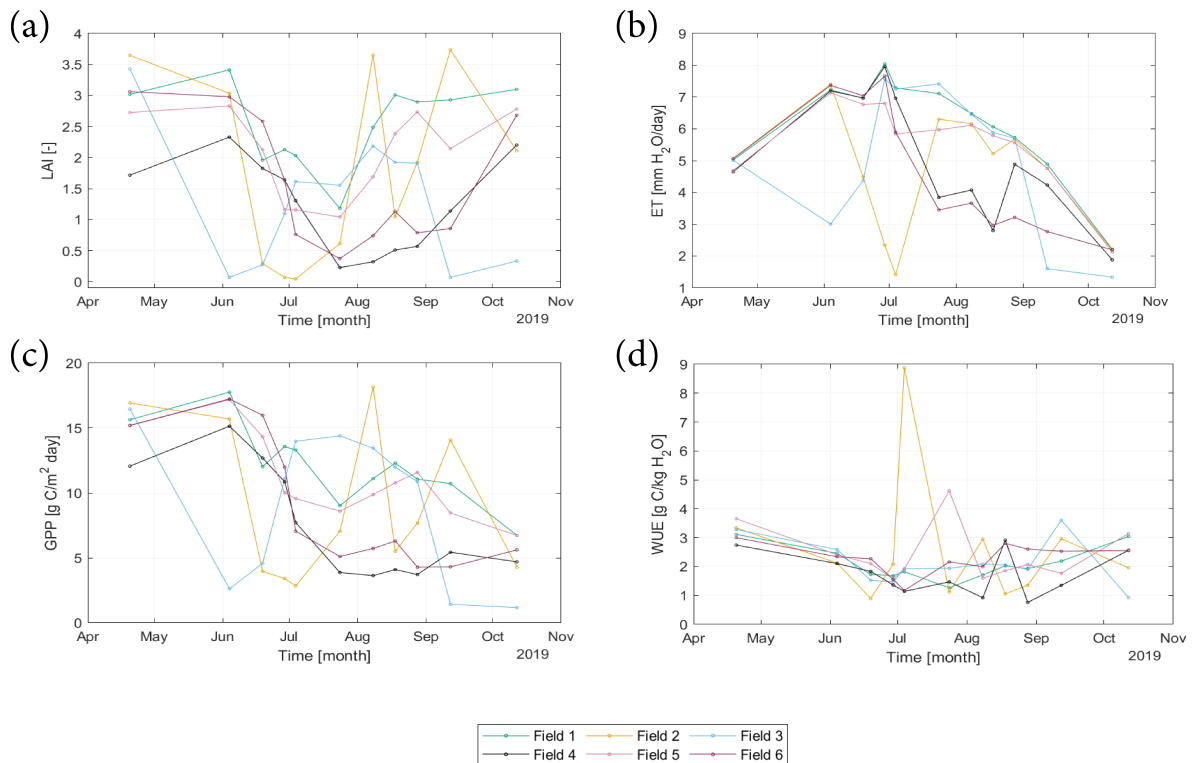


FIGURE A.1: Mean daily (a) leaf area index, (b) evapotranspiration, (c) gross primary production and (d) water use efficiency of the six used test fields in the study area.

Acknowledgements

It was a pleasure working with both my supervisor Eugénie and faculty member Alex during my Master's Thesis. Thank you Eugénie for helping me understand abstract concepts and supporting me in both a scientific and personal way. And thank you Alex for giving me the chance to write this thesis in your group in such short notice. The constructive feedback during the weekly staff meetings with the RSWs group was very appreciated and helped to overcome many hurdles. The in situ data was very kindly prepared and provided by Regine and Sabina from the Institute of Agricultural Sciences at ETH. A warm thank you also goes to the FlexSpace-Crew who was always around for a cup of coffee and long talks, which generated a lot of new ideas and inputs. And lastly, I would like to thank all my family and friends for supporting me during this time and for believing in me in times I could not.

Personal Declaration

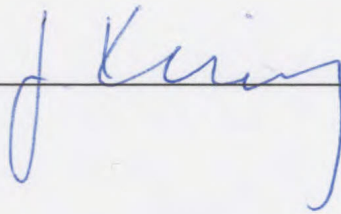
I hereby declare that the submitted thesis is the result of my own, independent work. All external sources are explicitly acknowledged in the thesis.

Date:

September 28, 2020

Signature

Jasmin Kesselring

A handwritten signature in blue ink, appearing to read 'J. Kesselring', is written over a solid horizontal black line. The signature is fluid and cursive.